Local Topology Inference of Mobile Robotic Networks under Formation Control

Yushan Li, Jianping He, Lin Cai, and Xinping Guan

Abstract—The interaction topology is critical for efficient cooperation of mobile robotic networks (MRNs). We focus on the local topology inference problem of MRNs under formation control, where an inference robot with limited observation range can manoeuvre among the formation robots. This problem faces new challenges brought by the highly coupled influence of unobservable formation robots, inaccessible formation inputs, and unknown interaction range. The novel idea here is to advocate a range-shrink strategy to perfectly avoid the influence of unobservable robots while filtering the input. To that end, we develop consecutive algorithms to determine a feasible constant robot subset from the changing robot set within the observation range, and estimate the formation input offline and the interaction range online. Then, an ordinary least squares based local topology estimator is designed with the previously inferred information. Resorting to the concentration measure, we prove the convergence rate and accuracy of the proposed estimator, taking the estimation errors of previous steps into account. Extensions on nonidentical observation slots and more complicated scenarios are also analyzed. Comprehensive simulation tests and method comparisons corroborate the theoretical findings.

I. Introduction

Mobile robotic networks (MRNs) have received increasing attention in the last decades. Thanks to the mobility, flexibility, and distributed fashion, MRNs are widely deployed, e.g., surveillance, reconnaissance, search and environmental monitoring [1]. Among these applications, formation control serves as a fundamental technique to enhance the cooperation performance by maintaining a preset geometric shape [2]. Numerous methods have been proposed to obtain stable and robust formation control, see [3], [4] for a detailed review. Despite the large variety of the control methods, the interaction topology among robots is universal and critical for effective cooperation of MRNs. The topology characterizes the locality of information exchange, and determines the shape-forming stability and convergence.

Recent years have witnessed the emergence of many applications that necessitate advances in topology inference, which provides key support to better understand and interact with the system. From the security perspective, the topology describing

Yushan Li, Jianping He, and Xinping Guan are with the Department of Automation, Shanghai Jiao Tong University, Shanghai 200240, China; Key Laboratory of System Control and Information Processing, Ministry of Education of China, Shanghai 200240, China; Shanghai Engineering Research Center of Intelligent Control and Management, Shanghai 200240, China (e-mail: yushan_li@sjtu.edu.cn; jphe@sjtu.edu.cn; xpguan@sjtu.edu.cn).

Lin Cai is with the Department of Electrical and Computer Engineering, University of Victoria, BC, Canada (email: cai@ece.uvic.ca).

the interactions of formation robots is extremely sensitive information in many military scenarios. External attackers can utilize the inferred topology to find the critical robot that has significant impacts in the formation, e.g., by calculating the node degree and centrality [5], or identifying the leadership relationship in the formation [6]. Following this, more intelligent attacks can be performed to interfere with the formation [7]–[10]. From the perspective of system flexibility, inferring the topology of formation can support the self-configuration of the robots based on their local interaction nature [11]. For instance, when a robot disconnects with others, it can use the inferred topology to maintain coordination by predicting the state and reconnecting with neighboring robots [12]. Even when the system scale becomes large and one can only have local topology information, the inferred local topology can still be leveraged to find the locally optimal node and implement the above tasks with locally optimal rewards.

Mathematically, topology inference can be seen as a typical inverse modeling problem. Plenty of related works have been developed for various dynamic models [13]–[15]. In relation to the basic consensus dynamics, the interaction topology is reconstructed by measuring the power spectral density of the network response to input noises in [16]. For sparsely connected dynamical networks, eigenvalue decomposition-based optimization methods in [17], [18] are proposed to reconstruct the topology. [19], [20] investigate the identifiability conditions of the system topology of a class of heterogeneous dynamical networks, from the perspective of characterizing the system transfer matrix from input to output. Despite the fruitful results, these methods cannot handle the topology inference of MRNs under formation control. For example, many well-established techniques are effective when the system is asymptotically stable and only involves zero-mean noises input [21], or the input is known [22], [23]. Nevertheless, in practical formation control, the input is generally regular, the system can be marginally stable, and the state is not always fully observable. In a word, careful treatments of the formation input, interaction characteristics and observation limitations are still lacking.

To fill the gap, this paper focuses on the local topology inference problem of MRNs under first-order linear formation control, where an inference robot can manoeuvre among the formation robots and observe their motions. Specifically, the inference robot has no knowledge of the formation input and interaction parameters, and the observation range is strictly limited. This problem is challenging due to three aspects. First, the set of robots within the observation range of the inference robot can change over time. Second, the movement

of formation robots heavily depends on the unknown formation input and interaction constraints. Third, the state evolution of the observable robot subset is determined by not only itself but also the unobservable robots. It is quite difficult to decouple the influences of the mixed three factors, and obtain a reliable local topology from the noise-corrupted observations. To address these issues, the key insight is to determine an available robot set from the changing observable robot set, and eliminate the influence of the unobservable robots. Then, we need to filter the influence of the formation input from local observations and design an unbiased topology estimator.

Preliminary results about estimator design with known interaction range have appeared in [24]. In this paper, we consider a more general situation where the interaction range is unknown, and extend the method design and performance analysis of the whole inference process. The main contributions are summarized as follows.

- We investigate the local topology inference problem of MRNs under noisy observations, without the knowledge about the formation input and interaction parameters. By characterizing the steady formation pattern, we determine a constant subset from the time-varying set of robots within the observation range, and identify the formation input parameters offline. The estimation error bound under finite observations is established in probability.
- Leveraging the interaction constraints between formation robots, we develop an active excitation based method to estimate the interaction range online. Combining the novel range-shrink strategy and the monotonicity analysis of the interaction range, the influence of unobservable robots is perfectly avoided. Then, an ordinary least squares (OLS) based local topology estimator is established after filtering the formation input's influence on the observations before the steady stage.
- The convergence and accuracy of the proposed estimator are proved, by resorting to the concentration measure with probability guarantees. Extensions on nonidentical observation slots of the robots and on more complicated control models are also discussed and analyzed. Simulation studies and comparison tests illustrate the effectiveness of the proposed method.

The remainder of this paper is organized as follows. Section II presents related literature. Section III gives the modeling for MRNs and formulates the inference problem. Section IV studies how to identify the steady pattern and interaction range. Section V develops the design of the local topology estimator and analyzes the inference performance. Simulation results are shown in Section VI, followed by the concluding remarks and further research issues in Section VII. All the proofs of theorems are provided in the Appendix.

II. RELATED WORK

Formation control in MRNs. The fundamental rules for formation control were first introduced by the famous Reynolds' Rules [25]: separation, alignment, and cohesion. Based on the rules, numerous methods have been proposed to achieve the desired performance, and consensus-based algorithms have become the mainstream, e.g., [26]–[28]. The key idea of consensus-based algorithms is that the formation is modeled as a graph, and every robot exchanges information (positions and velocities) with its neighbors and computes its control inputs. Therefore, the interaction structure lays critical support for effective formation control and is largely affected by communication network. In recent years, communication-free formation control [29]–[31] has been developed and attracts research interests, which avoids information delays and network bandwidth consumption in the interaction. For instance, formation control with bearing measurements by vision sensors was investigated in [32]. Note that in all cases, the interaction range is restricted by the physical distance between robots due to the energy constraints, i.e., two distant robots outside the interaction range are disconnected.

Topology Inference. A large body of research concerning topology inference has been developed in the literature. [33], [34] used Granger causality to formulate the directionality of the information exchange among system nodes, and constructed corresponding estimators to infer the underlying topology. Identifying the topology of sparsely connected networks via compressed sensing is also commonly investigated [35]–[38], which is transformed to a constrained L_1 norm optimization problem based on limited observations. Considering the latent regularity in the time series of nodal observations and adopting some basic assumptions (e.g., smoothness), graph signal processing methods [39]–[43] are proposed to derive a topology interpretation for the causation or correlation between nodes. When the network dynamics are nonlinear, kernel-based methods were developed to infer the topology [44]–[46]. The key idea is to select appropriate kernel functions to approximate the nonlinearities, where the performance is mainly determined by the kernel design. Several works [6], [23] have directly considered inferring the topology of MRNs, but they still lack performance guarantees, especially when the knowledge about the formation input is unavailable.

In summary, most existing works cannot directly infer the topology of MRNs under formation control, due to the unknown formation input and interaction characteristics. Despite many attempts on the asymptotic inference performance, there is no analytical model for the inference error under finite observations. These challenges motivate this paper.

III. PRELIMINARIES AND PROBLEM FORMULATION

Let $\mathcal{G} = (\mathcal{V}, \mathcal{E})$ be a directed graph that models an MRN, where $\mathcal{V} = \{1, \cdots, n\}$ is a finite set of nodes (i.e., robots) and $\mathcal{E} \subseteq \mathcal{V} \times \mathcal{V}$ is the set of interaction edges. An edge $(i, j) \in \mathcal{E}$ indicates that i will use the information from j. The adjacency matrix $A = [a_{ij}]_{n \times n}$ of $\mathcal{G}$ is defined such that $a_{ij} > 0$ if (i, j) exists, and $a_{ij} = 0$ otherwise. Denote $\mathcal{N}_i^{in} = \{j \in \mathcal{V} : a_{ij} > 0\}$ and $\mathcal{N}_i^{out} = \{j \in \mathcal{V} : a_{ji} > 0\}$ as the in-neighbor and out-neighbor sets of i, respectively.

Throughout the paper, we use the scripts $\tilde{\cdot}$ and $\hat{\cdot}$ right above a variable to indicate the corresponding observation and estimator, respectively. We denote by $\| \cdot \|$ the spectral norm and by $\| \cdot \|_F$ the Frobenius norm of a matrix. Denote $\mathbf{0}$ by all-zero matrix and $\mathbf{1}$ by all-one matrix in compatible dimensions.

TABLE I
SOME IMPORTANT NOTATION DEFINITIONS

Symbol	Definition
r_a, r_i	the abbreviation of the inference robot, robot i
z_k^a, z_k^i	the state of r_a, r_i at time k
$\mathbf{z}_k^a, \mathbf{z}_k^i$	the two-dimensional position of r_a, r_i at time k
c	the desired velocity of formation robots
h	the shape configuration vector of formation robots
k_s	the time when ϵ-steady pattern is reached
k_{end}	the time when r_a stops observation
$\mathcal{V}_F^a(k)$	the robot set within r_a's observation range at time k
$\mathcal{V}_F$	the constant robot subset observed by r_a
$\mathcal{V}_H$	the robot subset by range-shrink strategy ($\mathcal{V}_H \subseteq \mathcal{V}_F$)
z_k^F, z_k^H	the state vector of robot set $\mathcal{V}_F, \mathcal{V}_F$ at time k
W	the interaction topology matrix among the formation
W_{HF}	the interaction topology matrix between $\mathcal{V}_H$ and $\mathcal{V}_F$
R_f	the observation range of r_a
R_c	the interaction range of formation robots
R_o	the obstacle detection radius of formation robots
X	the matrix of k_s filtered observations about $\mathcal{V}_F$
Y	the matrix of k_s filtered observations about $\mathcal{V}_H$

The set variables are expressed in capital calligraphy fonts, and $\mathcal{V}_a \backslash \mathcal{V}_b$ represents the elements in $\mathcal{V}_a$ that are not in $\mathcal{V}_b$. The two-dimension state of a robot is expressed in boldface font (e.g., $\mathbf{z}$). Unless otherwise noted, the formulation with non-boldface state variables applies to the robot state in each dimension independently. For square matrices M_a and M_b in the same dimensions, $M_a \succeq M_b$ ($M_a \preceq M_b$) means $M_a - M_b$ is positive-semidefinite (negative-semidefinite). For two real-valued functions f_1 and f_2, $f_1(x) = \boldsymbol{O}(f_2(x))$ as $x \to x_0$ means $\lim_{x \to x_0} |f_1(x)/f_2(x)| < \infty$, and $f_1(x) = \boldsymbol{o}(f_2(x))$ as $x \to x_0$ means $\lim_{x \to x_0} |f_1(x)/f_2(x)| = 0$. Some important symbols are summarized in Table I.

A. Formation Control

To describe the predefined geometric shape under formation control, the shape vector $h_0 = [h_0^1, \cdots, h_0^n]^\mathsf{T}$ is introduced, where h_0^i ($i \in \mathcal{V}$) is the desired relative deviation between robot i (abbreviated to r_i hereafter) and a common reference point. To achieve this pattern, a common first-order discrete consensus-based controller is given by [47]

$$z^i(t_{k+1}) = z^i(t_k) + \varepsilon_\tau \sum_{j \in \mathcal{N}_i^{in}} a_{ij}(z^j(t_k) - z^i(t_k) - h_0^{ij}), \quad (1)$$

where $h_0^{ij} = h_0^j - h_0^i$ is desired state deviation between j and i, and $\varepsilon_\tau = t_{k+1} - t_k$ is the control period satisfying $\varepsilon_\tau \leq 1/\max\{d_i : i \in \mathcal{V}\}$. Note that once the formation shape is specified, the choice of the reference point will make no difference as h_0^{ij} remains unchanged.

Generally, to dynamically guide the formation motion, one robot will be specified as the leader with an extra velocity input. For simplicity and without loss of generality, r_n is taken as the leader and reference node, and suppose that it runs in a constant velocity c_0. Let $L = \text{diag}\{A\mathbf{1}_n\} - A$ be the Laplacian matrix of $\mathcal{G}$, and denote $u_0 = Lh_0 + [0, \cdots, 0, c_0]^\mathsf{T}$. Then, the global dynamics of the system is described by

$$z(t_{k+1}) = (I_n - \varepsilon_\tau L)z(t_k) + \varepsilon_\tau u_0 \triangleq Wz(t_k) + \varepsilon_\tau u_0, \quad (2)$$

where W equivalently represents the original topology matrix A and is known as Perron matrix. Apparently, W is row-stochastic, i.e., $W\mathbf{1}_n = \mathbf{1}_n$. For ease of notation, we denote $z_k \triangleq z(t_k)$, $c \triangleq \varepsilon_\tau c_0$, $h \triangleq \varepsilon_\tau h_0$ and $u \triangleq \varepsilon_\tau u_0$ in following sections. Then, (2) is rewritten as

$$z_{k+1} = Wz_k + u. \quad (3)$$

We make the following assumption throughout this paper.

Assumption 1 (System stability). *The eigenvalue 1 of W is simple (i.e., its algebraic multiplicity equals one), and the magnitudes of all other eigenvalues are less than one.*

B. Obstacle-avoidance and Interaction Constraints

The obstacle-avoidance mechanism is critical for MRNs to interact with the physical environment. Denote by R_o the obstacle detection range, and by $u_k^{j,e}$ the input triggered by the excitation source (i.e., the obstacle r_{ob}) on r_j. Once the relative distance between r_j and r_{ob} satisfies $\|\mathbf{z}^j - \mathbf{z}^{ob}\| \leq R_o$, the state of r_j is updated by

$$z_{k+1}^{j,e} = \sum_{\ell \in \mathcal{V}} w_{j\ell}(z_k^\ell - z_k^j) + u_k^j + u_k^{j,e}, \quad (4)$$

where the first two terms on the right hand side (RHS) can be seen as the internal interaction within the MRN, while the last term represents the external interaction with the environment.

There are numerous obstacle-avoidance algorithms in the literature (e.g., [48] provides a detailed review), and among them, $u_k^{j,e}$ is mainly determined by the desired goal state, the relative state and velocity between r_j and r_{ob}. As long as the excitation source appears within the obstacle-detection range of r_j, there will always be a $u_k^{j,e} \neq 0$. In this work, we do not specify the detailed form of $u_k^{j,e}$, but mainly leverage the obstacle-avoidance property that

$$|u_k^{j,e}| > 0, \text{ if } \|\mathbf{z}^j - \mathbf{z}^{ob}\| \leq R_o. \quad (5)$$

In practical applications, the interaction capability of robots is limited due to the energy constraint, and thus the interaction range among robots (denoted by R_c) is bounded [1], satisfying

$$R_o < R_c < \infty. \quad (6)$$

C. Problem of Interest

Suppose an inference robot (denoted by r_a) can manoeuvre in an MRN described by the formation control model (3). Specifically, r_a is equipped with advanced sensors with a limited observation range, and does not have knowledge about the formation input and interaction parameters. Note that both the formation robots and r_a are moving during the whole process, indicating that the robots within the observation range of r_a can change over time. Let $\mathcal{V}_F^a(k) \subseteq \mathcal{V}$ be the set of robots within r_a's observation range at time k, given by

$$\mathcal{V}_F^a(k) = \{i : \|\mathbf{z}_k^i - \mathbf{z}_k^a\|_2 < R_f\}, \quad (7)$$

where R_f is the observation range of r_a. Since there can be possible observation inaccuracies brought by the movement of robots, r_a's observation for $i \in \mathcal{V}_F^a(k)$ is described by

$$\tilde{z}_k^i = z_k^i + \omega_k^i, \ i \in \mathcal{V}_F^a(k), \quad (8)$$
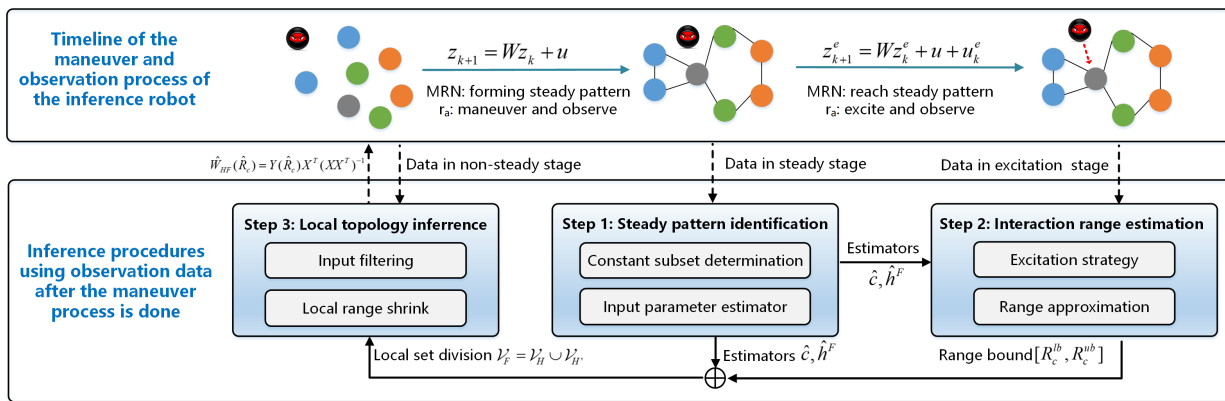
Fig. 1. The proposed local topology inference procedures. The estimator is established after the maneuver-observation process. First, the inference robot r_a estimates the formation input parameters c and h^F offline using the collected observations over the MRN. Then, r_a estimates the interaction range between two robots online, using data from the active excitation stage. Finally, with the estimated information, r_a can filter the influence of the unobservable part and determine the shrunken range. Specifically, the inferred topology can be leveraged in turn to approximate the best shrink and infer a new local topology.

where ω_k^i is the i-th element of *i.i.d.* Gaussian noise vector $\omega_k \in \mathbb{R}^n$, satisfying $\omega_k \sim N(0, \sigma^2 I)$. Considering the interaction constraint (6) in $\mathcal{V}$, we assume that R_f satisfies

$$R_f \geq R_c, \qquad (9)$$

which implicates that r_a can observe at least one single robot and all its in-neighbors.

The goal of this paper is to investigate how r_a can infer the local topology of the formation from the observations $\{\tilde{z}_k^i, \ i \in \mathcal{V}_F^a(k)\}$. This problem is very challenging, and most existing methods cannot be directly applied due to three factors: i) Time-varying $\mathcal{V}_F^a(k)$: the observations of robots in $\mathcal{V}_F^a(k)$ may be discontinuous and insufficient. ii) Weak prior knowledge: the unknown formation input and interaction parameters make direct inference from $\{\tilde{z}_k^i, i \in \mathcal{V}_F^a(k)\}$ unavailable. iii) Limited observation range: the neighbors that send real-time information to $\mathcal{V}_F^a(k)$ may locate outside the observation range of r_a. We will address these issues from the following aspects to obtain a reliable local topology inference.

- Utilizing the steady pattern of the formation, we first demonstrate how to determine a constant subset $\mathcal{V}_F \subseteq \mathcal{V}_F^a(k)$ as available inference sources, and identify the formation input from corresponding observations.
- Since the interaction range between robots is limited, we develop an excitation method to estimate the interaction range, and later use it to improve the local topology inference performance.
- Towards the influence of unobservable robots on $\mathcal{V}_F$, we propose a novel range-shrink method to guarantee that the inferred topology is unbiased in the asymptotic sense.

Based on the above treatments, we finally present the local topology estimator, along with its convergence and accuracy analysis. Specifically, the situation that the observation slots for robots in $\mathcal{V}_F$ are nonidentical will also be analyzed. The whole framework of this paper is shown in Fig. 1. Note that the final estimator is determined after the maneuver-observation process is done, and thus the sequence of the proposed inference steps is not necessarily aligned with the running sequence of the formation in the timeline.

IV. ESTIMATING THE STEADY PATTERN AND THE INTERACTION RANGE

In this section, we first demonstrate how to determine a constant subset $\mathcal{V}_F$ from $\mathcal{V}_F^a(k)$ and identify the formation input. Then, we present the range-shrink idea by introducing a common truncated estimator. Finally, the excitation strategy for estimating the interaction range is provided.

A. Determining Constant Robot Subset $\mathcal{V}_F$

Suppose the MRN starts the formation task from an arbitrary initial state. Given the initial position of r_a, r_a needs to manoeuvre among the formation robots and avoid collisions with them, namely, keeping $\|\mathbf{z}_k^a - \mathbf{z}_k^i\|_2 > R_o, i \in \mathcal{V}_F^a(k)$. This can be easily achieved by making r_a not too close to the robots and track the formation velocity, e.g., setting

$$u_k^a = \sum_{i \in \mathcal{V}_F^a(k)} (z_k^i - z_{k-1}^i)/|\mathcal{V}_F^a(k)| + g_a(\mathcal{V}_F^a(k)), \quad (10)$$

where $|\mathcal{V}_F^a(k)|$ represents the cardinality of $\mathcal{V}_F^a(k)$, $g_a(\mathcal{V}_F^a(k))$ represents the adjusting input when r_a is too close to some robots, and the sum term is for formation tracking. Note that any strategy that meets the above requirement can be adopted by r_a. Then, we focus on how to infer the local topology from r_a's observations in this process.

Since the steady pattern of the MRN reflects the formation shape and moving speed of the MRN, we first characterize the steady pattern by introducing the notion of linear steady trajectory, and determine the subset $\mathcal{V}_F$ to be inferred.

Definition 1 (Linear steady trajectory)**.** *Given the dynamic system (3), its state evolution $\{z_k\}$ is subject to linear steady trajectory if there exists unique $c \in \mathbb{R}$ and $s \in \mathbb{R}^n$ such that*

$$z_k = ck\mathbf{1}_n + s. \qquad (11)$$

By referring to the Theorem 1 in our preliminary work [24], we have the following result about the steady trajectory.

Lemma 1. *By the constant controller $u = Lh + [0 \cdots 0 \ c]^\mathsf{T}$, the system (3) will approximate the linear steady trajectory*

with arbitrary precision, i.e., given an arbitrary $\epsilon > 0$, there always exists a $k_0 \in \mathbb{N}^+$ and a $s \in \mathbb{R}^n$, such that

$$\|z_k - ck\mathbf{1}_n - s\|_1 < \epsilon, \forall k \geq k_0. \tag{12}$$

Lemma 1 illustrates that when the formation is in the linear steady trajectory with tolerant accuracy ϵ (we call it as ϵ-steady pattern hereafter), all robots are running at a common speed with fixed relative state deviations. Given appropriate moving strategies for r_a, e.g., by (10), we have the following result.

Lemma 2. *Given an arbitrary $\epsilon > 0$, there always exists a $k_1 \in \mathbb{N}^+$, such that $\mathcal{V}_F^a(k)$ remains unchanged $\forall k \geq k_1$.*

Lemma 2 follows easily from Lemma 1. Taking the moving strategy (10) as an example, when the formation reaches ϵ-steady pattern, r_a will also move stably with the MRN with almost the same velocity, and thus the formation robots in the observation range of r_a will not change. Based on this analysis, we determine the constant local subset $\mathcal{V}_F$ by

$$\mathcal{V}_F = \mathcal{V}_F^a(k_{end}), \tag{13}$$

where k_{end} represents the time when r_a stops observing the MRN. For simplicity, we temporarily assume $\mathcal{V}_F \subseteq \mathcal{V}_F^a(k)$ for an arbitrary k, and extend the analysis to the cases when this assumption is violated in Section V-E.

B. Steady Pattern Identification

After the local set $\mathcal{V}_F$ is determined, the steady pattern parameters of the formation can be identified from the observations by utilizing Lemma 1. Based on (12) and taking the observation noises into account, if the robots in $\mathcal{V}_F$ have reached ϵ-steady pattern, then the pattern parameters can be identified by solving

$$\min_{c,s^F} \sum_{t=k}^{k+L_c} \left\| \tilde{z}_t^F - ct\mathbf{1}_{n_f} + s^F \right\|_2^2, \tag{14}$$

where $\tilde{z}_t^F = [\tilde{z}_t^i, i \in \mathcal{V}_F] \in \mathbb{R}^{n_f}$ represents the observation vector of $\mathcal{V}_F$ at time t, $n_f = |\mathcal{V}_F|$, and L_c is the observation window length. Note that (14) is a typical least squares problem, whose solution is given by

- **Steady pattern estimator**:

$$\begin{cases} \hat{c}(k, L_c) = \sum_{t=k}^{k+L_c-1} \mathbf{1}_{n_f}^\mathsf{T}(\tilde{z}_{t+1}^F - \tilde{z}_t^F)/(n_f L_c), \\ \hat{s}^F(k, L_c) = \sum_{t=k+1}^{k+L_c}(\tilde{z}_t^F - \hat{c}t\mathbf{1}_{n_f})/L_c. \end{cases} \tag{15}$$

Next, we demonstrate the estimation performance of (15).

Theorem 1 (Accuracy of $\hat{c}$ and $\hat{s}^F$)**.** *Suppose the MRN has reached ϵ-steady pattern after k_0. Let $\Delta_c = \hat{c}(k_0, L_c) - c$ be the estimation error of $\hat{c}$, then we have*

$$\Pr\left\{|\Delta_c| \leq \frac{4\epsilon}{\sqrt{L_c}}\right\} \geq P_1(L_c), \tag{16}$$

where $P_1(L_c) = 1 - 2\exp\{-\frac{n_f L_c \epsilon^2}{\sigma^2}\}$. Denote the estimation error of $\hat{s}^F$ as $\Delta_s = \mathbf{1}_{n_f}^\mathsf{T}(\hat{s}^F(k_0, L_c) - s)/n_f$, then it satisfies

$$\lim_{L_c \to \infty} |\mathbb{E}[\Delta_s]| \leq 2\epsilon, \quad \lim_{L_c \to \infty} \mathbb{D}[\Delta_s] = \frac{\sigma^2}{2n_f}, \tag{17}$$

where $\mathbb{E}[\cdot]$ and $\mathbb{D}[\cdot]$ represent the expectation and variance of a random variable, respectively.

Proof. The proof is provided in Appendix A. $\qquad\square$

Theorem 1 demonstrates that, with sufficient observations over the ϵ-steady pattern, the estimation accuracy of $\hat{c}$ is determined by ϵ. In other words, the confidence interval of $\hat{c}(k_0, L_c)$ is given as $\hat{c}(k_0, L_c) \in [c - \frac{4\epsilon}{\sqrt{L_c}}, c + \frac{4\epsilon}{\sqrt{L_c}}]$ with probability at least $P_1(L_c)$. Specifically, when $L_c \to \infty$, we have with probability one that

$$\lim_{L_c \to \infty} |\Delta_c| = 0. \tag{18}$$

However, as for the estimation accuracy of $\hat{s}^F$, it only achieves ϵ-level accuracy in the expected sense with bounded variance.

Remark 1. *Note that (17) only presents the estimation error of $\hat{s}^F$ in limit form. It is shown in the proof of Theorem 1 that, one has with high probability*

$$\begin{cases} |\mathbb{E}[\Delta_s]| \leq (2 + \dfrac{2k_0+1}{L_c})\epsilon, \\ \mathbb{D}[\Delta_s] = \dfrac{\sigma^2}{2n_f} + \sigma^2(\dfrac{1}{n_f L_c^2} + \dfrac{(2k_0+1)^2}{L_c^2} + \dfrac{4k_0+2}{L_c}). \end{cases} \tag{19}$$

Despite the undesired uncertainty in Δ_s, one can tighten the error bound of $\hat{s}^F(k, L_c)$ by using more observations.

Note that (15) is not an appropriate solution if the system is not in ϵ-steady pattern. Hence, we need to judge whether the system is in ϵ-steady pattern before obtaining the final $\hat{c}$ and $\hat{s}$. Inspired by (16), we in turn deduce that $|\Delta_c| > 4\epsilon/\sqrt{L_c}$ holds with high probability if the observations used are not all in ϵ-steady pattern. Hence, we use the last L_c groups of observation to obtain a benchmark estimator of c by

$$\hat{c}_b \overset{\Delta}{=} \hat{c}(k_{end} - L_c, L_c). \tag{20}$$

Based on Theorem 1, if the system is in ϵ-steady pattern after k_0, one has with probability $1 - 2\exp\{-\frac{n_f L_c \epsilon^2}{\sigma^2}\}$ that

$$\begin{aligned} |\hat{c}(k_0, L_c) - \hat{c}_b| &\leq |\hat{c}(k_0, L_c) - c| + |c - \hat{c}_b| \\ &\leq 8\epsilon/\sqrt{L_c}. \end{aligned} \tag{21}$$

Although infinite observations are not available in practice, the upper bound in (21) can be used as an empirical criterion to judge when the ϵ-steady pattern is reached, given by

- **ϵ-steady time criterion**:

$$k_s = \inf\{k : |\hat{c}(k, L_c) - \hat{c}_b| \leq 8\epsilon/\sqrt{L_c}\}. \tag{22}$$

Once k_s is obtained, the two input parameters, the velocity c and the shape vector of $\mathcal{V}_F$, h^F, are finally determined by

$$\begin{cases} \hat{c} = \hat{c}(k_s, L_s), \\ \hat{h}^F = \hat{s}^F(k_s, L_s) - \mathbf{1}_{n_f}\hat{s}^i(k_s, L_s), \end{cases} \tag{23}$$

where $L_s = k_{end} - k_s$ represents the amount of observations of the system in the ϵ-steady stage.

C. Range-shrink: Motivated by Truncated Estimator

To explicitly illustrate the necessity of the range-shrink strategy, we begin with the case where the observations are noise-free and the input is known. Under full observation, denote $z_{k+1}^u \overset{\Delta}{=} z_{k+1} - u_k = W z_k$. Then, the global topology can be obtained from K groups of noise-free observations by

$$W = Z_{2:K+1}^u Z_{1:K}^{\mathsf{T}} (Z_{1:K} Z_{1:K}^{\mathsf{T}})^{-1}, \tag{24}$$

where $Z_{2:K+1}^u = [z_2^u, z_3^u, \cdots, z_{K+1}^u]$ and $Z_{1:K} = [z_1, z_2, \cdots, z_K]$. Note that the feasibility of the estimator under full observations relies on the invertibility of $(Z_{1:K} Z_{1:K}^{\mathsf{T}})$, which is related to the number of observations and the steady pattern of the formation. Here we temporarily suppose the invertibility holds, and analyze the details in the proposed local topology estimator in Section V-A.

Let $W_{FF} = [w_{ij}, \ i, j \in \mathcal{V}_F] \in \mathbb{R}^{n_f \times n_f}$ be the topology matrix of $\mathcal{V}_F$. To infer W_{FF} from $\{z_k^F\}$, it is certainly free for one to adopt a truncated form of (24) as in [49]

$$\hat{W}_{FF} = Z_{2:K+1}^{u,F} (Z_{1:K}^F)^{\mathsf{T}} (Z_{1:K}^F (Z_{1:K}^F)^{\mathsf{T}})^{-1}. \tag{25}$$

The works [21], [49], [50] have explored the conditions of using the truncated estimator to approximate the ground truth[1]. Nevertheless, these conditions are not consistent with our problem setting, and $\hat{W}_{FF}$ is far away from the ground truth from basic linear algebra, i.e.,

$$\hat{W}_{FF} \neq [Z_{2:K+1}^u Z_{1:K}^{\mathsf{T}} (Z_{1:K} Z_{1:K}^{\mathsf{T}})^{-1}]_{FF}. \tag{26}$$

More precisely, let $\mathcal{V}_{F'} = \mathcal{V} \backslash \mathcal{V}_F$ and the formation dynamics (3) can be divided into

$$\begin{bmatrix} z_{k+1}^F \\ z_{k+1}^{F'} \end{bmatrix} = \begin{bmatrix} W_{FF} & W_{FF'} \\ W_{F'F} & W_{F'F'} \end{bmatrix} \begin{bmatrix} z_k^F \\ z_k^{F'} \end{bmatrix} + \begin{bmatrix} u_k^F \\ u_k^{F'} \end{bmatrix}, \tag{27}$$

where $z_k^{F'}$ is the state of $\mathcal{V}_{F'}$ at time k. Substituting $\tilde{z}_k^F = z_k^F + \omega_k^F$ into (27), the observation of $\mathcal{V}_F$ is given by

$$\tilde{z}_{k+1}^F = W_{FF} \tilde{z}_k^F + u_k^F + W_{FF'} z_k^{F'} + \omega_{k+1}^F - W_{FF} \omega_k^F. \tag{28}$$

Note that (28) only represents the explicit relationship of every two consecutive observations, not a real process. It is clear that the unobserved and non-negligible term $\{W_{FF'} z_k^{F'}\}$ incurs the inequality of (26), making it extremely hard to obtain an unbiased estimator of W_{FF} from noisy $\{\tilde{z}_k^F\}$.

Thanks to the constrained interaction characteristics of MRNs, we observe that the robots that are outside r_i's interaction range have no influence on r_i. Therefore, we transform the inference objective by shrinking the inference scope from $\mathcal{V}_F$ to a smaller $\mathcal{V}_H$, which directly avoids the inference bias in the truncated estimator (25). As shown in Fig. 2, we use a concentric circle to cover the feasible subset $\mathcal{V}_H \subseteq \mathcal{V}_F$ with radius R_h, satisfying

$$R_h = R_f - R_c. \tag{29}$$

---

[1]In [21], [49], [50], the conditions of using estimator (25) are summarized as: i) the topology is in symmetric Erdős-Rényi random graph form with vanishing connection probability, and ii) the ratio of the observable nodes to all nodes converges to constant as the size of the network goes to infinity.
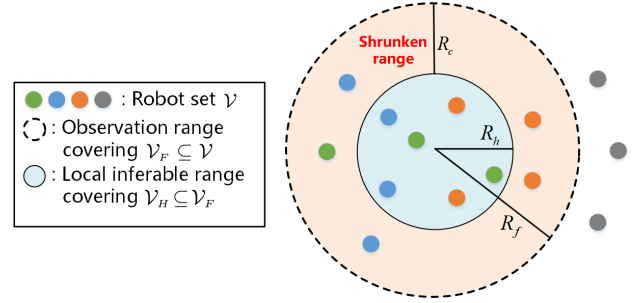

Fig. 2. Illustration of observation ranges. The blue circle area enclosing $\mathcal{V}_H$ is with radius R_h, and larger circle area enclosing $\mathcal{V}_F$ is with radius R_f.

Once the subset $\mathcal{V}_H$ is determined, we can design an unbiased estimator of the following local topology,

$$W_{HF} = [w_{ij}, \ i \in \mathcal{V}_H, j \in \mathcal{V}_F] \in \mathbb{R}^{n_h \times n_f}, \tag{30}$$

where $n_h = |\mathcal{V}_H|$. Note that W_{HF} covers all connections within $\mathcal{V}_H$ and the directed connections from $\{\mathcal{V}_F \backslash \mathcal{V}_H\}$ to $\mathcal{V}_H$. The details are presented in the next section.

D. Inferring Interaction Range by Active Excitation

Next, we present the active excitation based method to illustrate how to estimate the interaction radius R_c.

Note that robots are equipped with sensors to detect obstacles around. When r_a is very close to r_j, by the obstacle-avoidance rule (4), an excitation input will be triggered in r_j. Then, the observed state of r_j under excitation is given by

- **Observation under excitation**:

$$\tilde{z}_k^{j,e} = ck + s^j + \epsilon_k^j + \omega_k^j + u_{k-1}^{j,e}, \tag{31}$$

where ϵ_k^j is the j-th element of $\epsilon_k = z_k - ck\mathbf{1}_n - s$, which represents the residual error vector with the linear steady trajectory. According to Lemma 1, when the MRN is in ϵ-steady pattern, $\|\epsilon_k\|_1 \leq \epsilon$. Next, we present the details of the active excitation based method as follows.

- *Step 1: Initial excitation on r_j.*

Based on (31) and recalling the velocity estimation error Δ_c, the velocity prediction error on $j \in \mathcal{V}$ at the ϵ-steady pattern is calculated by

$$\begin{aligned} \delta_k^j &= \tilde{z}_k^{j,e} - \tilde{z}_{k-1}^j - \hat{c} \\ &= (\omega_k^j - \omega_{k-1}^j) + (\epsilon_k^j - \epsilon_{k-1}^j) - \Delta_c + u_{k-1}^{j,e}. \end{aligned} \tag{32}$$

Note that δ_k^j is a random variable, and $u_{k-1}^{j,e} = 0$ if r_j is not excited. Based on Theorem 1, if r_j is under no excitation, then we have $|\delta_k^j| \leq \sqrt{3\epsilon^2 + 2\sigma^2}$ with a high probability. Utilizing this empirical result, we design the following criterion to determine whether r_j is excited by r_a and its reaction range (i.e., the obstacle detection range R_o), given by

$$\begin{cases} k_e = \inf\{k : |\delta_k^j| > \sqrt{3\epsilon^2 + 2\sigma^2}\}, \\ \hat{R}_o = \|\mathbf{z}_{k_e}^j - \mathbf{z}_{k_e}^a\|_2, \end{cases} \tag{33}$$

where k_e is the starting moment of the excitation stage.

- *Step 2: Excitation strategy.*

This article has been accepted for publication in IEEE Transactions on Automatic Control. This is the author's version which has not been fully edited and content may change prior to final publication. Citation information: DOI 10.1109/TAC.2023.3237484

7

To keep r_a within the obstacle detection range of r_j, we define the feasible state set of r_a as

$$\mathcal{Z}_{k+1}^a = \{\mathbf{z}_{k+1}^a : \|\mathbf{z}_{k+1}^a - \hat{\mathbf{z}}_{k+1}^j\|_2 \le \hat{R}_o\}, \quad (34)$$

For better identification, the next movement of r_a is randomly selected from $\mathcal{Z}_{k+1}^a$ in the same direction, i.e.,

$$\mathbf{z}_{k+1}^a \in \mathcal{Z}_{k+1}^a \cap \{\mathbf{z}_{k+1}^a : z_{k+1}^a \cdot z_k^a \ge 0 \text{ in each dimension}\}. (35)$$

- *Step 3: Estimating R_c based on out-neighbors.*

If r_j is injected with the excitation input $u_{k-1}^{j,e}$, the influence of $u_{k-1}^{j,e}$ will spread to $\mathcal{N}_j^{out}$ in following moments. Suppose r_a makes excitations over r_j for consecutive m time steps, then the accumulated velocity prediction error of $i \in \mathcal{N}_j^{out}$ in the m-step is calculated by

$$\delta_{k+m,k}^i = \tilde{z}_{k+m}^{i,e} - \tilde{z}_k^i - m\hat{c}. \quad (36)$$

Next, we define the following out-neighbor estimation function and demonstrate its accuracy.

Definition 2 (Out-neighbor indicator)**.** *The indicator of the event that $i \in \mathcal{N}_j^{out}$, Θ_{ij}, is defined as*

$$\Theta_{ij} = \begin{cases} 1, & \text{if } w_{ij} > 0, \\ 0, & \text{otherwise.} \end{cases} \quad (37)$$

The estimator of Θ_{ij} is defined as

$$\hat{\Theta}_{ij} = \begin{cases} 1, & \text{if } |\frac{\delta_{k+m}^i}{m}| > (\frac{4}{\sqrt{L_c}} + \frac{4}{\sqrt{m}})\epsilon, \\ 0, & \text{otherwise.} \end{cases} \quad (38)$$

Theorem 2 (Accuracy of $\hat{\Theta}_{ij}$)**.** *Under m consecutive excitations on r_j, the true positive probability of estimator $\hat{\Theta}_{ij}$ is lower bounded as*

$$\Pr\left\{\Theta_{ij} = 1 | \hat{\Theta}_{ij} = 1\right\} \ge P_1(L_c) \cdot P_2(m), \quad (39)$$

where $P_2(m) = 1 - 2\exp\{-\frac{m\epsilon^2}{\sigma^2}\}$.

Proof. The proof is provided in Appendix B. □

Theorem 2 demonstrates that by active excitations, the out-neighbors of r_j (within the observation range) can be determined with a high probability. Besides, if there exists at least one out-neighbor of r_j in $\mathcal{V}_F$, then the two robots are always within the interaction range during the whole process. Utilizing this characteristic, we take the maximum distance between r_j and the inferred r_j's out-neighbors from their observations as the lower bound of R_h, given by

$$R_c^{lb} = \sup\left\{\|\tilde{\mathbf{z}}_t^i - \tilde{\mathbf{z}}_t^j\|_2 : \hat{\Theta}_{ij} = 1, t = 1, \cdots, k_e + m\right\}. \quad (40)$$

The procedures of obtaining R_c^{lb} are summarized in Algorithm 1. Then, the interaction range satisfies

$$R_c^{lb} \le R_c \le R_c^{ub}, \quad (41)$$

where $R_c^{ub} = R_f$. The range interval (41) is critical for final topology inference.

Algorithm 1 Infer the interaction range R_c

Input: Steady moment k_s, excitation number m, $\hat{c}$ and $\hat{h}$.
Output: Lower bound of R_c.
1: Select a excitation target $j \in \mathcal{V}_F$;
2: **while** $|\delta_k^j| \le \sqrt{3\epsilon^2 + 2\sigma^2}$ **do**
3:    r_a moves closer to r_j, $k = k + 1$;
4: **end while**
5: $k_e = k$, $\hat{R}_o = \|\mathbf{z}_{k_e}^j - \mathbf{z}_{k_e}^a\|_2$;
6: **for** $t = 1 \to m$ **do**
7:    Update $\mathbf{z}_{k_e+t}^a$ by (35);
8: **end for**
9: **for** all $i \in \mathcal{V}_F \backslash \{j\}$ **do**
10:    **if** $|\frac{\delta_{k+m}^i}{m}| > (\frac{4}{\sqrt{L_c}} + \frac{4}{\sqrt{m}})\epsilon$ **then**
11:      $\hat{\Theta}_{ij} = 1$;
12:    **end if**
13: **end for**
14: **if** all $\hat{\Theta}_{ij} = 0$ **then**
15:    re-select a target robot and go to line 2;
16: **end if**
17: Compute R_c^{lb} by (40);

V. ESTIMATOR DESIGN AND PERFORMANCE ANALYSIS

By the methods proposed in the last section, the obtained estimators of $\hat{c}$, $\hat{h}^F$ and $\hat{R}_c^{lb}$ make the local topology inference feasible. However, directly using $\hat{R}_c^{lb}$ to determine $\mathcal{V}_H$ is relatively conservative. In this section, we first present the estimator of local topology W_{HF} and leverage it to reversely approximate R_c. Then, taking the estimation error of $\hat{c}$ and $\hat{h}^F$ into consideration, we give the non-asymptotic error bound of $\|\hat{W}_{HF} - W_{HF}\|$. Finally, we demonstrate how to utilize the knowledge acquired in the active excitation stage to improve further the inference performance based on $\hat{W}_{HF}$.

A. Local Topology Inference under Given R_c

First, we analyze the inference performance of the ordinary least squares estimator under a given interaction range R_c. If R_c is determined, the inferable subset $\mathcal{V}_H \subseteq \mathcal{V}_F$ is also determined by $R_h = R_f - R_c$. Considering the possibility that the formation leader $r_n \in \mathcal{V}_F$, we need to discriminate its influence. Given $\mathcal{V}_F$ and k_s, if the leader $r_n \in \mathcal{V}_F$, then it is identified by

$$\hat{r}_n = \arg\min_i \left\{f_c^i : f_c^i \le \frac{8\epsilon}{\sqrt{L_c}}, i \in \mathcal{V}_F\right\}, \quad (42)$$

where $f_c^i = |\sum_{k=0}^{k_s-1}(\tilde{z}_{k+1}^i - \tilde{z}_k^i - \hat{c}_b)|/k_s$. Note that if $\hat{r}_n$ is empty, it means $r_n \notin \mathcal{V}_F$. To discriminate this situation, we define the indicative leader vector $\mathbb{I}_F$ by

$$\mathbb{I}^F(i) = \begin{cases} 1, & \text{if } \exists i \in \mathcal{V}_F, i = \hat{r}_n, \\ 0, & \text{otherwise.} \end{cases} \quad (43)$$

Next, we will illustrate how to filter the influence of the input to infer the local topology, and use it to approximate the real

R_c. Let $\mathcal{V}_{H'} = \mathcal{V}_F \backslash \mathcal{V}_H$ and $W_{HF} = [W_{HH} \; W_{HH'}]$. Define two variables of filtered $\tilde{z}_k^F$ and organize them as

$$
\begin{aligned}
x_k &= (\tilde{z}_k^F - \hat{h}^F) \in \mathbb{R}^{n_f}, \\
y_k &= (\tilde{z}_k^H - \hat{h}^H - \hat{c}\mathbb{I}^H) \in \mathbb{R}^{n_h}, \\
X &= [x_0, x_1, \cdots, x_{k_s-1}] \in \mathbb{R}^{n_f \times k_s}, \\
Y &= [y_1, y_2, \cdots, y_{k_s}] \in \mathbb{R}^{n_h \times k_s}.
\end{aligned}
\tag{44}
$$

Then, by referring to Theorem 2 in our preliminary work [24], we present the following local topology estimator.

Theorem 3. *Given the filtered observation matrices X and Y, and supposing R_c is known, if $k_s \geq |\mathcal{V}_F|+1$, then the optimal estimation of W_{HF} in the sense of least squares is*

$$
\hat{W}_{HF} = YX^{\mathsf{T}}(XX^{\mathsf{T}})^{-1}.
\tag{45}
$$

Theorem 3 gives the least squares solution of W_{HF} when R_c is known. The core insight is that by the range-shrink strategy, the truncated state $[Wx]^H = W_{HF}x^F$, which perfectly avoids the influence brought by the unobservable $\mathcal{V}_{F'}$. Although the number of feasible observations is limited in practice, Theorem 3 can be used as the basis for approximating W_{HF} from noisy observations.

Remark 2. *Note that the invertibility of XX^{T} is guaranteed by two aspects: the used observations from the non-steady stage and the random observation noises. First, the observation matrix X consists of k_s groups of observations before the ϵ-steady pattern is reached. These informative observations reflect the transient phase of the formation from the initial state to the steady pattern, and are the key to inferring the underlying topology. To ensure the informativity, i.e., the minimal observation number condition $k_s \geq |\mathcal{V}_F|+1$ in Theorem 3, the initial state of the formation cannot be set such that it is too close with the preset shape (if so, the inference robot can interfere with formation to make it deviate from the preset shape), while the topology matrix W satisfies Assumption 1. Second, the observations $\{\tilde{z}_k^F\}$ are corrupted by independent random noises. According to Sard's theorem in measure theory, X has full rank almost surely. In other words, the random noises further enhance the invertibility of XX^{T} with the informativity guaranteed, and together effectively avoid the ill-posedness of the estimator.*

B. Convergence of the Proposed Estimator

Next, we focus on the convergence performance of $\hat{W}_{HF}$ assuming R_c is known. Taking the estimation error of $\hat{c}$ and $\hat{h}^F$ into account, the convergence of $\hat{W}_{HF}$ is characterized by the following result.

Theorem 4 (Convergence of $\hat{W}_{HF}$ with known R_c). *Let $P_3(k_s) = 1 - 2\exp\{-(k_s + n_h)\}$ and suppose R_c is known. With probability at least $P_1(L_c) \cdot P_3(k_s)$, the error of the topology estimator $\hat{W}_{HF}(\hat{R}_c)$ satisfies*

$$
\|\hat{W}_{HF} - W_{HF}\| = \boldsymbol{O}(\frac{1}{k_s}) + \boldsymbol{o}(\frac{1}{k_s^2}).
\tag{46}
$$

Proof. The proof is provided in Appendix C. □

Theorem 4 demonstrates the convergence rate of $\hat{W}_{HF}$ in terms of k_s in probability. Apparently, if the observations before the ϵ-steady pattern are sufficient, then $\hat{W}_{HF}$ will closely approximate the ground truth in a rate of $\frac{1}{k_s}$, satisfying

$$
\Pr\left\{\lim_{L_c, k_s \to \infty} \|\hat{W}_{HF} - W_{HF}\| = 0\right\} = 1.
\tag{47}
$$

Remark 3. *Note that since $\hat{W}_{HF}$ is based on the estimators $\hat{c}$ and $\hat{h}^F$, the bound of $\|\hat{W}_{HF} - W_{HF}\|$ is also related to ϵ, σ and L_c. In the proof of Theorem 4, we show that the RHS in (46) is in fact composed of multiple factors, including $\boldsymbol{O}(\frac{\epsilon}{k_s\sqrt{L_c}})$, $\boldsymbol{O}(\frac{\epsilon}{k_s})$, $\boldsymbol{O}(\frac{\sigma}{k_s})$ and $\boldsymbol{o}(\frac{\sigma^2}{k_s^2})$. Hence, we can characterize the bound as a uniform one about k_s. It is worth noting that, although the estimation errors of $\hat{c}$ and $\hat{h}^F$ are influenced by ϵ and σ, these parts of errors will have a slight influence on the accuracy of $\hat{W}_{HF}$ as k_s grows.*

Note that there are some possible techniques to further alleviate the influence of the observation noises, e.g., by de-regularization. In this method, the optimization objective is $\sum_{k=1}^{k_s} \|y_k^B - W_{HF}y_{k-1}^A\|^2 - \beta\|W_{HF}\|_F^2$, where $\beta > 0$ and the second negative term is called de-regularization term. Deeper investigation towards this direction will be left as future work.

C. Accuracy Analysis

It is illustrated in Theorem 4 that if the interaction range R_c is known, the local topology estimator $\hat{W}_{HF}$ converges to W_{HF} asymptotically. However, we only have an estimation range of R_c, i.e., $[R_c^{lb}, R_c^{ub}]$, and different $\hat{R}_c$ renders different cardinality of $\mathcal{V}_H$. To analyze the accuracy of the local topology inference under various $\hat{R}_c$, we explicitly write the local topology estimator as $\hat{W}_{HF}(\hat{R}_c)$, and propose a range approximation algorithm to find appropriate $\hat{R}_c$.

First, we use the maximum range R_c^{ub} to determine an auxiliary robot set $\mathcal{V}_{H_0} \subseteq \mathcal{V}_F$, which is covered by a concentric circle of r_a's observation range, with radius R_{h0} satisfying

$$
R_{h0} = R_f - R_c^{ub}.
\tag{48}
$$

Let $\mathcal{V}_{F_0}$ be the set of robots within the concentric circle range with radius $(R_{h0} + \hat{R}_c)$, and denote $\mathcal{V}_{F_0'} = \mathcal{V}_F \backslash \mathcal{V}_{F_0}$. Note that here $\mathcal{V}_{H_0}$ is constant and $\mathcal{V}_{F_0}$ will change with $\hat{R}_c$. Apparently, we have $\mathcal{V}_{H_0} \subseteq \mathcal{V}_{F_0} \subseteq \mathcal{V}_F$ and $\mathcal{V}_{H_0} \cap \mathcal{V}_{F_0'} = \emptyset$. For the robots in $\mathcal{V}_{F_0'}$, r_a will regard that $\hat{w}_{ij}(\hat{R}_c) = 0$, $i \in \mathcal{V}_{H_0}, j \in \mathcal{V}_{F_0'}$. For the robots in $\mathcal{V}_{F_0}$, $\hat{W}_{H_0F_0}(\hat{R}_c)$ is computed by the OLS estimator. Combining the two parts, W_{H_0F} is estimated by

$$
\hat{W}_{H_0F}(\hat{R}_c) = \left[Y_{H_0}X_{F_0}^{\mathsf{T}}(X_{F_0}X_{F_0}^{\mathsf{T}})^{-1}, \mathbf{0}_{|\mathcal{V}_{H_0}| \times |\mathcal{V}_{F_0'}|}\right].
\tag{49}
$$

Recall $\hat{W}_{H_0F}(\hat{R}_c)$ utilizes k_s groups of observations, and we define the following evaluation function of $\hat{R}_c$ to describe its influence on $\hat{W}_{H_0F}(\hat{R}_c)$

- **Asymptotic inference bias of $\hat{W}_{H_0F}(\hat{R}_c)$:**

$$
f_w(\hat{R}_c) = \lim_{k_s \to \infty} \|\hat{W}_{H_0F}(\hat{R}_c; k_s) - W_{H_0F}\|.
\tag{50}
$$

This article has been accepted for publication in IEEE Transactions on Automatic Control. This is the author's version which has not been fully edited and content may change prior to final publication. Citation information: DOI 10.1109/TAC.2023.3237484

9

Algorithm 2 search_suboptimal_$R_c(R_c^{ub}, R_c^{lb}, n_c, n_w)$

Input: Range $[R_c^{lb}, R_c^{ub}]$, decision threshold ε_w, counting number n_c and stopping threshold n_w.

Output: Suboptimal estimation of R_c.

1: $\hat{R}_c = (R_c^{ub} + R_c^{lb})/2$;
2: Determine the subset $\mathcal{V}_{F_0}$ by $R_{f0} = R_{h0} + \hat{R}_c$;
3: Compute $f_e(\hat{R}_c)$ by (53);
4: **if** $f_e(\hat{R}_c) > \varepsilon_w$ **then**
5:     $R_c^{lb} = \hat{R}_c$, $n_c = 1$;
6:     search_suboptimal_$R_c(R_c^{ub}, R_c^{lb}, n_c, n_w)$;
7: **else**
8:     $R_c^{ub} = \hat{R}_c$, $n_c = n_c + 1$;
9:     **if** $n_c \geq n_w$ **then**
10:       Return R_c^{ub};
11:     **else**
12:       search_suboptimal_$R_c(R_c^{ub}, R_c^{lb}, n_c, n_w)$;
13:     **end if**
14: **end if**

Theorem 5 (Inference bias under different $\hat{R}_c$)**.** *The asymptotic inference bias $f_w(\hat{R}_c)$ is monotonically decreasing w.r.t. the inferred range $\hat{R}_c$ in probability, i.e., if $\hat{R}_{c1} \geq \hat{R}_{c2}$,*

$$\Pr\left\{ f_w(\hat{R}_{c1}) \leq f_w(\hat{R}_{c2}) \right\} = 1. \tag{51}$$

Specifically, if $\hat{R}_c \geq R_c$, the estimator $\hat{W}_{H_0F}(\hat{R}_c)$ is asymptotically unbiased, i.e.,

$$\Pr\left\{ f_w(\hat{R}_c) = 0 \right\} = 1. \tag{52}$$

Proof. The proof is provided in Appendix D. $\square$

Theorem 5 demonstrates the decreasing monotonicity of $f_w(\hat{R}_c)$ in asymptotic sense. Note that $\hat{R}_c \geq R_c$ is a sufficient condition to guarantee an asymptotically unbiased $\hat{W}_{H_0F}(\hat{R}_c)$. Despite not knowing the real R_c and W_{H_0F} in practice, from Theorem 5 we deduce that $f_w(R_c^{ub}) = f_w(R_c) = 0$, which indicates that $\hat{W}_{H_0F}(R_c^{ub})$ can be leveraged to replace $W_{H_0F}(R_c)$ for evaluation. Accordingly, we define the empirical bias of $\hat{W}_{H_0F}(\hat{R}_c)$ as

- **Empirical inference bias of** $\hat{W}_{H_0F}(\hat{R}_c)$:

$$f_e(\hat{R}_c) = \|\hat{W}_{H_0F}(\hat{R}_c) - \hat{W}_{H_0F}(R_c^{ub})\|. \tag{53}$$

Based on (53), we propose Algorithm 2 to obtain a suboptimal estimation of R_c from the range $[R_c^{lb}, R_c^{ub}]$. The key idea of the algorithm is to validate the monotonicity of $f_e(\hat{R}_c)$, and find an appropriate $\hat{R}_c$, such that $f_e(\cdot)$ remains stable even when $\hat{R}_c$ increases. Specifically, the classic bisection method is used to speed up the search efficiency and a decision threshold ε_w and a stopping threshold n_w are introduced to terminate the process. Note that the larger ε_w and smaller n_w are, the more conservative $\hat{R}_c$ is.

Remark 4. *Our previous assumption about i.i.d. Gaussian noises can be relaxed on independent but non-identical cases, i.e., $\mathbb{E}[\omega_t \omega_s^\mathsf{T}] = \delta_{ts} \,\mathrm{diag}(\sigma_{\omega_1}^2, \sigma_{\omega_2}^2, \cdots, \sigma_{\omega_n}^2)$. The key insight is to adopt $\max\{\sigma_{\omega_1}^2, \sigma_{\omega_2}^2, \cdots, \sigma_{\omega_n}^2\}$ as the variance bound for all observation noises in the analysis. Although the upper*

bound of the error $\|\hat{W}_{HF} - W_{HF}\|$ during analysis process becomes conservative, this scaling step does not invalidate the asymptotic accuracy of $\hat{W}_{HF}$ when $k_s \rightarrow \infty$, i.e., $\lim_{k_s \to \infty} \|\hat{W}_{HF} - W_{HF}\| = 0$ still holds with a convergence rate of $\boldsymbol{O}(\frac{1}{k_s})$. If one specifically focuses on the minimal error bound performance under finite samples, the analysis can be carried out using the concentration inequality and state-of-the-art system identification methods (e.g., see [51], [52]).

D. Estimator Design with Its Improved Solution

With the ϵ-steady pattern parameter $\hat{c}$, $\hat{h}^F$ and interaction range $\hat{R}_c$ (output of Algorithm 2) determined, we are able to design the unbiased topology estimator of W_{HF} with the maximum number of robots. Consequently, the set $\mathcal{V}_H$ is in turn specified by $R_h = R_f + \hat{R}_c$. Then, the local topology W_{HF} is estimated by

$$\hat{W}_{HF}(\hat{R}_c) = Y(\hat{R}_c)X^\mathsf{T}(XX^\mathsf{T})^{-1}. \tag{54}$$

Despite the asymptotic boundedness of the OLS estimator (54), the proposed method nevertheless can be used as the basis for inferring the local topology when a finite number of observations are available.

Note that (54) only utilizes $\hat{R}_c$ to specify the inference scope of $\mathcal{V}_H$. In fact, $\hat{R}_c$ can be regarded as the prior knowledge that r_a has mastered in the excitation stage to further improve the inference accuracy. The key insight is that two robots that are not within range R_c will not receive information from each other. Leveraging this as a hard constraint, $\hat{W}_{HF}$ can be further optimized by solving the following problem

$$\min_{W_{HF}} \quad \|Y(\hat{R}_c) - W_{HF}X\|_{\mathrm{Fro}}^2 \tag{55a}$$

$$\text{s.t.} \quad w_{ij} = 0, \text{if } \|\tilde{\mathbf{z}}^i - \tilde{\mathbf{z}}^j\|_2 > \hat{R}_c, i \in \mathcal{V}_H, j \in \mathcal{V}_F. \tag{55b}$$

Note that (55) is a typical constrained linear least squares problem, and can be solved by many mature optimization techniques, e.g., interior-point method [53].

Finally, we briefly summarize how the local topology W_{HF} is inferred from noisy observations $\{\tilde{z}_k^i, i \in \mathcal{V}_F^a(k)\}_{k=1}^{k_{end}}$. The first step is to determine the constant subset $\mathcal{V}_F$ and estimate the input parameters from the observations in steady pattern. Then, the interaction range between robots is estimated. Utilizing the range-shrink strategy and estimated interaction range, we further determine the appropriate subset $\mathcal{V}_H$. At last, the local topology is inferred by (45) and its improved version (55), where the input's influence on the non-steady observations $\{\tilde{z}_k^F\}_{k=1}^{k_s}$ is filtered.

E. Extensions and Discussions

Recall that the topology estimator is obtained by solving $\min_{W_{HF}} \|Y - W_{HF}X\|_F^2$. In fact, it can be decomposed into inferring the rows of W_{HF} independently, i.e., solving

$$\min_{W_{HF}^{[i,:]}} \|Y^{[i,:]} - W_{HF}^{[i,:]}X\|^2, \tag{56}$$

for all $i \in \mathcal{V}_H$. Based on this decomposition, we demonstrate how to infer the local topology when $\mathcal{V}_F \subseteq \mathcal{V}_F^a(k)$ does not always hold.

Note that if there exists $k < k_{end}$ such $\mathcal{V}_F \not\subset \mathcal{V}_F^a(k)$, it indicates that the observation range of r_a does not cover robots in $\mathcal{V}_F$ simultaneously. Let the starting time that $i \in \mathcal{V}_F$ be

$$k_f^i = \inf \left\{ k_\ell : i \in \bigcap_{k=k_\ell}^{k_{end}} \mathcal{V}_F^a(k) \right\}. \qquad (57)$$

Next, as indicated in (55), if r_j is outside the interaction range of r_i, then the interaction weight $w_{ij} = 0$. This property further relaxes the dependence on the observations of $\mathcal{V}_F$. For an explicit expression, denote by $\tilde{\mathcal{V}}_F^i$ the robot set that has possible influences on r_i, given by

$$\tilde{\mathcal{V}}_F^i = \{j : j \in \mathcal{V}_F \text{ and } \|\tilde{\mathbf{z}}_{k_{end}}^j - \tilde{\mathbf{z}}_{k_{end}}^i\|_2 \leq \hat{R}_c\}. \qquad (58)$$

Apparently, one has $i \in \tilde{\mathcal{V}}_F^i \subseteq \mathcal{V}_F$. Recalling the filtered observation variables defined in (44), we permutate the filtered observations of $\tilde{\mathcal{V}}_F^i$ and the local topology matrix associated with r_i as follows,

$$\tilde{X}_i = [\tilde{x}_{k_f^i}(i), \tilde{x}_{k_f^i+1}(i), \cdots, \tilde{x}_{k_s-1}(i)] \in \mathbb{R}^{|\tilde{\mathcal{V}}_F^i| \times (k_s - k_f^i)},$$

$$\tilde{Y}_i = [y_{k_f^i+1}^i, y_{k_f^i+1}^i, \cdots, y_{k_s}^i] \in \mathbb{R}^{1 \times (k_s - k_f^i)},$$

$$\tilde{W}_i = [(w_{ij}, j \in \tilde{\mathcal{V}}_F^i)_{1 \times |\tilde{\mathcal{V}}_F^i|}, \mathbf{0}_{1 \times (n_f - |\tilde{\mathcal{V}}_F^i|)}] \in \mathbb{R}^{1 \times |\tilde{\mathcal{V}}_F^i|},$$

where $\tilde{x}_k(i) = [x_k^\ell]_{\ell \in \tilde{\mathcal{V}}_F^i}$ is the partitioned part in x_k that corresponds to $\tilde{\mathcal{V}}_F^i$. Based on the above formation, the following result is presented to illustrate how to infer the local topology W_{HF} row-by-row.

Corollary 1. *Given the observations before ϵ-steady time k_s. For r_i, if $|\tilde{\mathcal{V}}_F^i| \leq k_s - k_f^i$, then its associated local topology $\tilde{W}_i$ can be uniquely inferred by*

$$\hat{\tilde{W}}_i = [\tilde{Y}_i \tilde{X}_i^{\mathsf{T}} (\tilde{X}_i \tilde{X}_i^{\mathsf{T}})^{-1}, \mathbf{0}_{1 \times (n_f - |\tilde{\mathcal{V}}_F^i|)}]. \qquad (59)$$

The proof of this corollary is the same as that of Theorem 3, and the details are omitted here. From Corollary 1, the available observation slot for inferring r_i's local topology $\tilde{W}_i$ is not necessarily the same as that of other robots in $\mathcal{V}_F$. Besides, $\hat{\tilde{W}}_i$ is the optimal estimation of $\tilde{W}_i$ in the sense of least squares, as long as the observation slot satisfies $|\tilde{\mathcal{V}}_F^i| \leq k_s - k_f^i$. Similar to the convergence and accuracy of $\hat{W}_{HF}$, $\hat{\tilde{W}}_i$ enjoys the convergence of $O(\frac{1}{k_s - k_f^i})$ and the asymptotical accuracy when $k_s \to \infty$.

In summary, although the integrated estimator $\hat{W}_{HF}$ can be unavailable if robots in $\mathcal{V}_H$ occur in r_a's observation range at different moments, one can still utilize Corollary 1 to infer the local topology associated with each $i \in \mathcal{V}_H$. Finally, the underlying W_{HF} is recovered by appropriately permuting the robot indexes of $\{\hat{\tilde{W}}_i, i \in \mathcal{V}_H\}$, and stacking them into one matrix row-by-row.

Remark 5. *The proposed inference method in this paper, which takes the first-order linear formation control as the entry point, also provides insights to tackle some second-order and nonlinear cases. Taking the second-order linear model in [54] as an example, the major difference here is that the topology matrix to be inferred describes the element-to-element interaction connections between both the positions and velocities of robots. The proposed method can be extended*
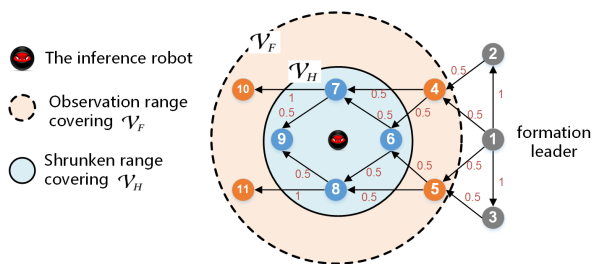

Fig. 3. An MRN of 11 robots and the interaction weights are in red font. Robot 1-3 are unobservable to r_a, robot 4-11 constitute the observable set $\mathcal{V}_F$, and robot 7-9 constitute the ideal subset $\mathcal{V}_H$.
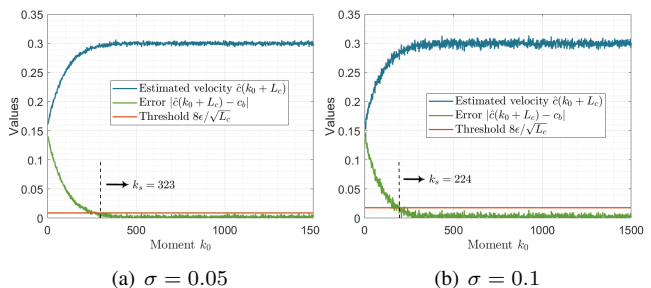

(a) $\sigma = 0.05$ (b) $\sigma = 0.1$

Fig. 4. Estimation of the formation speed $\hat{c}(k, L_c)$. The threshold parameter ϵ is set as $\epsilon = 0.8\sigma$.

to the second-order cases because the global state evolution shares the same linear form as that of the first-order case, with appropriate notations and treatments of the double dimensions for each robot. Besides, for a common class of nonlinear models like $z_{k+1}^i = z_k^i + \sum_{j=1}^n w_{ij} \varphi_{ij}(z_k^j - z_k^i - h^{ij})$ (where $\varphi_{ij}(\cdot)$ is the continuous and strictly-bounded nonlinear interaction function satisfying $\varphi_{ij}(y) = 0$ if $y = 0$), one can still use the proposed linear estimator to infer the underlying binary adjacent topology, combined with popular clustering methods as [49] does.

In many cases, it is also desirable to infer a sparse topology when the network size is large or the connections among nodes are sparsely distributed [37], [55], [56]. In this regard, we can modify the proposed method by adding an L_1-norm regularization term in the objective function (56) to enforce the sparsity, which is formulated as

$$\min_{W_{HF}^{[i,:]}} \|Y^{[i,:]} - W_{HF}^{[i,:]} X\|^2 + \alpha \|W_{HF}^{[i,:]}\|_1, \qquad (60)$$

where $\alpha > 0$ is the regularization parameter. Note that this problem is convex and can be efficiently solved using many mature optimization algorithms, e.g., [57], [58]. Finally, organize the solutions of the above problem for $i \in \mathcal{V}_H$ in an appropriate order, and the sparse estimation of W_{HF} is obtained.

VI. SIMULATION

A. Simulation Setting

In this section, we conduct numerical experiments to demonstrate the feasibility of inferring the local topology of the MRN, and validate the theoretical results. For simplicity, we consider a representative case of an MRN consisting of 11 robots. The preset formation shape and the robot set division are shown in Fig. 3. Specifically, robot 1 is set as the leader,
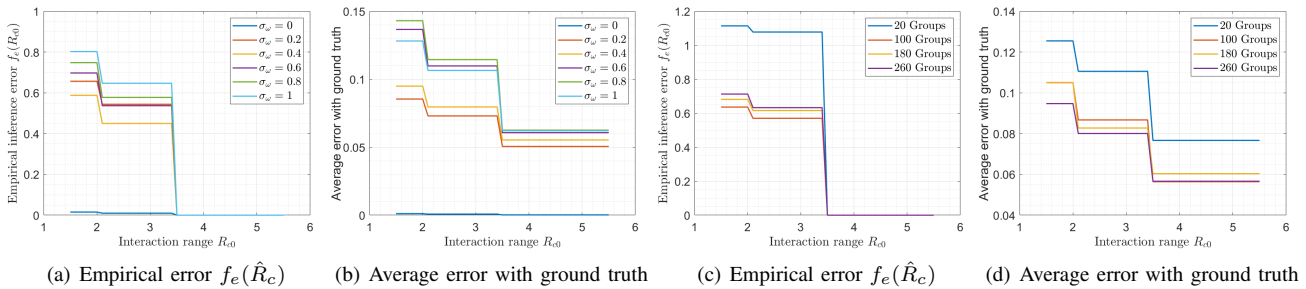
(a) Empirical error $f_e(\hat{R}_c)$ (b) Average error with ground truth   (c) Empirical error $f_e(\hat{R}_c)$ (d) Average error with ground truth

Fig. 5. Inference error of $\hat{W}_{H_0F}(\hat{R}_c)$. (a)(b): under different noise variance using 200 observations. (c)(d): under different observation amount with $\sigma = 0.4$.

(a) Under different noise   (b) Under different observation amount
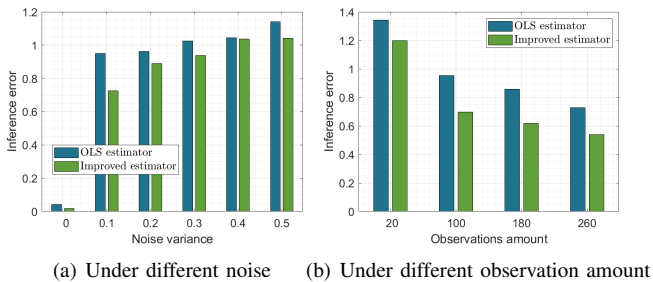
Fig. 6. Comparisons of inference error of OLS estimator $\hat{W}_{HF}(\hat{R}_c)$ and the improved estimator. 200 observations are used in (a), and $\sigma = 0.1$ in (b).

(a) Under different noise   (b) Under different observation amount
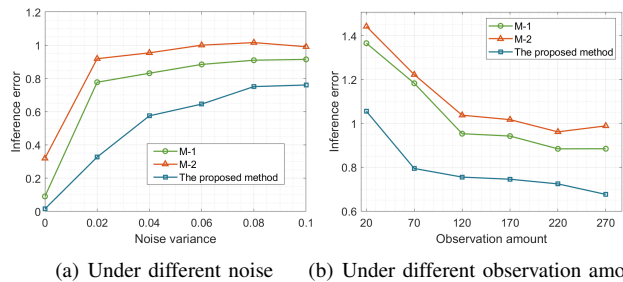
Fig. 7. Comparisons of the proposed method with methods in [21] (M-1) and [23] (M-2). 200 observations are used in (a), and $\sigma = 0.1$ in (b).

and the moving speed in stable stage is set as 0.3m/s. The observation range of r_a is set as $R_f = 9$m, and the interaction and obstacle-detection radius of a formation robot are set as $R_c = 5$m and $R_o = 1.5$m, respectively. The observation window length L_c is set to be 500. In the following parts, we will present the inference results of the steady pattern, the interaction range and the local topology.

B. Simulation Results

Let us begin with examining the steady pattern estimator (15) in terms of $\hat{c}(k, L_c)$. For simplicity, we set the threshold parameter $\epsilon = 0.8\sigma$, and conduct two groups of experiments using different σ. As shown in Fig. 4, when the MRN reaches the steady state, the velocity estimation remains stable. Specifically, the red line illustrates how to find the ϵ-steady time by the bound $8\epsilon/\sqrt{L_c}$ in (22). Apparently, the larger ϵ is set, the more conservative $\hat{c}(k, L_c)$ is.

Next, as shown in Fig. 5, the inference performance of the interaction range is evaluated. Since the active excitation method mainly aims to obtain a lower bound of $\hat{R}_c$, here we omit the simulation process of this stage and directly present the inference error under different $\hat{R}_c$. For fair comparisons, Fig. 5(a)-5(b) depict the error curve under noise variance from 0 to 1 using 200 observations, while Fig. 5(c)-5(d) depict the error curve under observation amount from 20 to 260 with $\sigma = 0.4$. Note that the average error of the inferred topology with the ground truth is computed as $\|\hat{W}_{H_0F}(\hat{R}_c) - W_{H_0F}\|/(|\mathcal{V}_H||\mathcal{V}_F|)$. As we can see, the empirical inference function $f_e(\hat{R}_c)$ and the average error are generally decreasing with $\hat{R}_c$. This corresponds to the result of Theorem 5 and supports the feasibility of using Algorithm 2 to determine a more accurate $\hat{R}_c$. Specifically, the more observations are involved, the smaller the average inference error w.r.t. the ground truth is.

Then, with $\hat{R}_c = 4.5$m, we compare the inference performance without and with the interaction constraint, corresponding to $\hat{W}_{HF}(\hat{R}_c)$ and (55), respectively. Fig. 6(a) presents the inference errors under different variances of observation noises, varying from 0 to 0.5. Each test is based on 200 observations over the same time window. Fig. 6(b) presents the inference errors under different number of observations, ranging from 20 to 260, with $\sigma = 0.1$. Note that all the error indexes (Y-coordinate) in the figures describe the absolute deviation between two variables instead of the relative. Under the same observation amount, the larger σ is, the less improvement can be obtained. When k_s and σ are not very large, remarkable improvements in the inference performance can be achieved. In addition, as shown in Fig. 6(b), the inference error can be further reduced with a larger available observation amount (i.e., k_s), which corresponds to the conclusion of Theorem 4.

Finally, we present the performance comparison of the proposed approach with the methods in [21] and [23] (denoted as M-1 and M-2, respectively), under the same settings of $\hat{R}_c$, noise variance and observation amount as the last experiment. Note that for fair comparisons, we use the filtered observations to implement M-1. Fig. 7(a) shows the relationships between the inference error and the observation noise variance for all methods. Fig. 7(b) shows the relationships between the inference error and the observation amount for all methods, under common noise variance $\sigma = 0.1$. It is clear from the presented results that the proposed method outperforms the other two, which mainly results from the estimation of the formation input and the interaction range. We also observe that the reason for M-1 having better performance than M-2 lies in the filtered observations we used. More detailed technical comparisons along with some other inference algorithms are summarized in Table II, which shows that the proposed method has better applicability and inference performance guarantees for the considered problem.

TABLE II
COMPARISONS OF THE PROPOSED METHOD WITH OTHER METHODS

Method	Topology Structure		Input Consideration		Local Inference		Input Filtering	Observation Noise	Convergence Speed
	Undirected	Directed	Random	Non-random	Feasibility	Conditions			
Truncated estimator in [21]	✓		✓		✓	Erdős-Rényi graph $\frac{N_O}{N} \in (0,1] (N \to \infty)$[1]			$\boldsymbol{O}(\sqrt{\frac{1}{T}})$[2]
Spectral method in [59]	✓		✓						$\boldsymbol{O}(e^{-L})$[3]
Geometric method in [6]		✓		✓	Binary judgement[4]	Non-steady trajectory is available		✓	No guarantee
OLS-based method in [23]		✓		✓	Feasible if revised[5]	Non-steady trajectory is available		✓	No guarantee
Our method		✓		✓	✓	Non-steady trajectory is available	✓	✓	$\boldsymbol{O}(\frac{1}{T})$

[1] N_O and N represent the cardinality of the observable subset and the whole node set, respectively.   [2] T here refers to the number of observations in the non-steady stage, and the system in this reference is asymptotically stable.   [3] In [59] the authors implement L groups of tests over the system, with the same initial state while ending at different moments, and no noise terms are involved.   [4] The method is based on the geometric characteristics of the robot trajectory. Although not tailored for the local topology inference of MRNs, we point out it can apply to infer whether the connection between two robots exists.   [5] The method is originally designed for global topology inference, and can be revised for the local cases if using the idea in this paper.

VII. CONCLUSION

In this paper, we have studied the problem of inferring the local topology of MRNs under first-order formation control, without the knowledge about formation input and interaction parameters. To overcome the inference challenges brought by the unknown formation input and interaction range, we first demonstrated how to determine the available robot subset for inference, considering the set of robots that are within the observation range of the inference robot might change over time. Then, we designed ϵ-steady pattern estimators to obtain the input parameters and an active excitation method to estimate the interaction range. Also, we proposed a range-shrink strategy to avoid the inference brought by the unobservable robots and presented the local topology estimator. The convergence rate and the accuracy of the proposed estimator were proved. Extensions on different observation slots for the robots and more complicated control models were also analyzed. Finally, extensive simulation tests and comparisons verified the effectiveness of the proposed method.

Future directions include i) generalizing the method to more complex formation control cases (e.g., switching topology and nonlinear dynamics); ii) investigating the possible attack against the MRNs based on the inferred topology along with its countermeasures.

ACKNOWLEDGEMENT

APPENDIX

A. Proof of Theorem 1

Proof. Based on Lemma 1, when the MRN has reached ϵ-steady pattern after k_0, the dynamics (3) is equivalent to

$$z_k^F = ck\mathbf{1}_{n_f} + s^F + \boldsymbol{\epsilon}_k^F, \tag{61}$$

where $\boldsymbol{\epsilon}_k = W^k z_0 + \left(\sum_{t=0}^{k-1} W^t\right) u - ck\mathbf{1}_n - s$, satisfying $\|\boldsymbol{\epsilon}_k\|_1 \leq \epsilon$. Then, the estimation error of $\hat{c}(k_0, L_c)$ is given by

$$
\begin{aligned}
\Delta_c &= \hat{c}(k_0, L_c) - c = \sum_{t=k_0}^{k_0+L_c-1} \sum_{i \in \mathcal{V}_F} \frac{(\tilde{z}_{t+1}^i - \tilde{z}_t^i - c)}{n_f L_c} \\
&= \sum_{t=k_0}^{k_0+L_c-1} \sum_{i \in \mathcal{V}_F} \frac{(\boldsymbol{\epsilon}_{t+1}^i - \boldsymbol{\epsilon}_t^i + \omega_{t+1}^i - \omega_t^i)}{n_f L_c} \\
&= \sum_{i \in \mathcal{V}_F} \frac{(\boldsymbol{\epsilon}_{k_0+L_c}^i - \boldsymbol{\epsilon}_{k_0}^i + \omega_{k_0+L_c}^i - \omega_{k_0}^i)}{n_f L_c}.
\end{aligned} \tag{62}
$$

For ease notation, define

$$
\begin{cases}
\bar{\epsilon}_c = \sum_{i \in \mathcal{V}_F} (\boldsymbol{\epsilon}_{k_0+L_c}^i - \boldsymbol{\epsilon}_{k_0}^i)/(n_f L_c), \\
\bar{\omega}_c = \sum_{i \in \mathcal{V}_F} (\omega_{k_0+L_c}^i - \omega_{k_0}^i)/(n_f L_c),
\end{cases} \tag{63}
$$

Then, we only need to prove the upper bound of $\Delta_c = \bar{\omega}_c + \bar{\epsilon}_c$.

Note that $\omega_k^i \sim N(0, \sigma^2)$ i.i.d., and thus $\bar{\omega}_c$ is subject to $N(0, 2\sigma^2/(n_f L_c^2))$. Based the Gaussian nature, one can obtain the following concentration inequality by finding the optimal Chernoff bound of $\bar{\omega}_c$ (see *example 2.1* in [60]), i.e.,

$$\Pr\{|\bar{\omega}_c| \leq \frac{2\epsilon}{\sqrt{L_c}}\} \geq 1 - 2\exp\{-\frac{n_f L_c \epsilon^2}{\sigma^2}\} = P_1(L_c). \tag{64}$$

As for $|\bar{\epsilon}_c|$, since the system is in ϵ-steady pattern, one has

$$|\bar{\epsilon}_c| \leq 2\epsilon/L_c \leq 2\epsilon/\sqrt{L_c}. \tag{65}$$

Hence, combining (64) and (65) yields that

$$\Pr\left\{|\bar{\epsilon}_c| + |\bar{\omega}_c| \leq \frac{4\epsilon}{\sqrt{L_c}}\right\} \geq P_1(L_c). \tag{66}$$

Substituting the absolute inequality $|\Delta_c| \leq |\bar{\omega}_c| + |\bar{\epsilon}_c|$ into (66), the first statement (16) is proved.

Next, consider the estimation error of $\hat{s}^F(k; L_c)$. Based on (61), one has

$$\hat{s}^F(k_0, L_c) - s^F = \sum_{t=k_0+1}^{k_0+L_c} (\boldsymbol{\epsilon}_t^F + \omega_t^F - \Delta_c t \mathbf{1}_{n_f})/L_c, \quad (67)$$

Similar with Δ_c, the average estimation of all elements in (67) is given by

$$\Delta_s = \frac{\mathbf{1}_{n_f}^\mathsf{T} \boldsymbol{\epsilon}_s}{n_f} + \frac{\mathbf{1}_{n_f}^\mathsf{T} \omega_s}{n_f} - \frac{\Delta_c(2k_0 + L_c + 1)}{2}, \qquad (68)$$

where $\boldsymbol{\epsilon}_s = \sum_{t=k_0+1}^{k_0+L_c} \boldsymbol{\epsilon}_t^F/L_c$ and $\omega_s = \sum_{t=k_0+1}^{k_0+L_c} \omega_t^F/L_c$. Taking $\bar{\epsilon}_c$ and $\bar{\omega}_c$ into the third term $\frac{\Delta_c(2k_0+L_c+1)}{2}$, one obtains

$$\frac{\Delta_c(2k + L_c + 1)}{2} = (\bar{\epsilon}_c + \bar{\omega}_c)(2k_0 + L_c + 1)/2. \quad (69)$$

Substituting (69) into (68), then one has $\Delta_s = \bar{\epsilon}_s + \bar{\omega}_s$ where

$$\begin{cases} \bar{\epsilon}_s = \dfrac{\mathbf{1}_{n_f}^\mathsf{T} \boldsymbol{\epsilon}_s}{n_f} + \dfrac{(2k_0 + L_c + 1)\bar{\epsilon}_c}{2}, \\ \bar{\omega}_s = \dfrac{\mathbf{1}_{n_f}^\mathsf{T} \omega_s}{n_f} + \dfrac{(2k_0 + L_c + 1)\bar{\omega}_c}{2}. \end{cases}$$

Utilizing $|\bar{\epsilon}_c| \leq 2\epsilon/L_c$ and $\omega_k^i \sim N(0, \sigma^2)$, one deduces that

$$|\bar{\epsilon}_s| \leq (2 + \frac{2k_0 + 1}{L_c})\epsilon, \tag{70}$$

$$\mathbb{D}[\bar{\omega}_s] = \frac{\sigma^2}{n_f L_c^2} + \frac{\sigma^2}{2n_f}(1 + \frac{(2k_0+1)^2}{L_c^2} + \frac{4k_0+2}{L_c}). \tag{71}$$

Combining (70) and (71), it yields that $\mathbb{E}[|\bar{\epsilon}_s| + \bar{\omega}_s] = |\bar{\epsilon}_c|$ and $\mathbb{D}[|\bar{\epsilon}_s| + \bar{\omega}_s] = \mathbb{E}[\bar{\omega}_s]$ holds. When $L_c \to \infty$, the second statement (17) is proved. $\qquad \square$

B. Proof of Theorem 2

Proof. To begin with, similar with (32), the accumulated velocity prediction error $\delta_{k+m,k}^i$ is expanded as

$$\delta_{k+m,k}^i = \sum_{t=1}^m w_{ij}^{(t)} u_{k+m-t-1}^{j,e} - m\Delta_c \\ + \omega_{k+m}^i - \omega_{k+1}^i + \boldsymbol{\epsilon}_{k+m}^i - \boldsymbol{\epsilon}_{k+1}^i, \qquad (72)$$

where $w_{ij}^{(t)}$ represents the t-power of w_{ij}.

Then, it follows that the average velocity prediction error in the m-period is given by

$$\frac{\delta_{k+m,k}^i}{m} = \frac{1}{m} \sum_{t=1}^m w_{ij}^{(t)} u_{k+m-t-1}^{j,e} - \Delta_c \\ + \frac{\omega_{k+m}^i - \omega_{k+1}^i}{m} + \frac{\boldsymbol{\epsilon}_{k+m}^i - \boldsymbol{\epsilon}_{k+1}^i}{m}. \qquad (73)$$

Note that $\frac{\omega_{k+m}^i - \omega_{k+1}^i}{m}$ is subject to $N(0, 2\sigma^2/m^2)$. Applying the Chernoff concentration inequality, one obtains

$$\Pr\left\{ \frac{|\omega_{k+m}^i - \omega_{k+1}^i|}{m} \leq \frac{2\epsilon}{\sqrt{m}} \right\} \geq 1 - 2\exp\{-\frac{m\epsilon^2}{\sigma^2}\} = P_2(m). \tag{74}$$

Recall that it is proved that $\Pr\left\{|\Delta_c| \leq 4\epsilon/\sqrt{L_c}\right\} \geq P_1(L_c)$ in Theorem 1, and $|\frac{\boldsymbol{\epsilon}_{k+m}^i - \boldsymbol{\epsilon}_{k+1}^i}{m}| \leq \frac{\epsilon}{m} \leq \frac{\epsilon}{\sqrt{m}}$ always holds. Combining these pieces, if r_j is under no excitation (i.e., $u^{j,e} = 0$), it yields that

$$\Pr\left\{ \frac{|\delta_{k+m}^i|}{m} \leq (\frac{4}{\sqrt{L_c}} + \frac{4}{\sqrt{m}})\epsilon \right\} \geq P_1(L_c) \cdot P_2(m). \quad (75)$$

Taking the converse-negative version of the statement (i.e., if $u^{j,e} = 0$ then (75) holds), it yields the statement described by (39). The proof is completed. $\qquad \square$

C. Proof of Theorem 4

Proof. For notational brevity, let $u_\Delta = \hat{h}^H - h^H + (\hat{c} - c)\mathbb{I}^H$ be the error vector of the filtered input. Then, for each pair of (y_k, x_k), we have

$$y_k = W_{HF} x_k + (W_{HH} - I_{n_h})u_\Delta + \omega_{k+1}^H - W_{HF}\omega_k^F. \quad (76)$$

Let $U_\Delta = [u_\Delta, \cdots, u_\Delta] \in \mathbb{R}^{n_h \times k_s}$, $\Omega^- = [\omega_0, \cdots, \omega_{k_s-1}]$ and $\Omega^+ = [\omega_1, \cdots, \omega_{k_s}]$. Then, all the filtered observations can be compactly written as

$$Y = W_{HF} X + (W_{HH} - I_{n_h})U_\Delta + \Omega_H^+ - W_{HF}\Omega_F^-. \quad (77)$$

Based on the estimator (45), the inference error matrix of $\hat{W}_{HF}$ is given by

$$\begin{aligned} & \|\hat{W}_{HF} - W_{HF}\| \\ =& \|((W_{HH} - I_{n_h})U_\Delta + \Omega_H^+ - W_{HF}\Omega_F^-)X^\mathsf{T}(XX^\mathsf{T})^{-1}\| \\ \leq& (\|(W_{HH} - I_{n_h})U_\Delta X^\mathsf{T}\| + \|(\Omega_H^+ - W_{HF}\Omega_F^-)X^\mathsf{T}\|)\|(XX^\mathsf{T})^{-1}\|. \end{aligned}$$
$$(78)$$

Next, we will prove that each term of the RHS of (78) is bounded individually.

- *Part 1: Upper Bounding $\|(XX^\mathsf{T})^{-1}\|$.*

Recall that the system state can be expanded recursively as

$$z_{k+1} = W^{k+1}z_0 + \left(\sum_{t=0}^k W^t\right)Lh + \left(\sum_{t=0}^k W^t\right)u_c \\ = c(k+1)\mathbf{1}_n + W^{k+1}z_0 + \sum_{t=0}^k (\sum_{i=2}^n \lambda_i^t q_i v_i^\mathsf{T})u. \qquad (79)$$

Note that the last two terms in the RHS of (79) is strictly bounded regardless of the moment k, and the influence of the independent observation noises will not accumulate during the state evolution. Since the term $c(k+1)\mathbf{1}_n$ takes the dominant role in the state evolution, we can directly characterize $\|X\|$ in terms of the time horizon k_s.

Based on the matrix norm inequality $\|X\| \leq \|X\|_F \leq \sqrt{\min\{n_h, k_s\}}\|X\|$, one easily infers that

$$\frac{\|X\|_F}{\sqrt{\min\{n_h, k_s\}}} \leq \|X\| \leq \|X\|_F. \tag{80}$$

Further utilizing $\|z_t z_t^\mathsf{T}\|_F = \boldsymbol{O}(t^2)$ and $\sum_{t=0}^{k_s} t^2 = k_s(k_s + 1)(2k_s + 1)/6$, one deduces that $\|\sum_{t=0}^{k_s} z_t z_t^\mathsf{T}\|_F = \boldsymbol{O}(k_s^3)$. Then, it follows that

$$\|X\| = \boldsymbol{O}(k_s^{3/2}), \|XX^\mathsf{T}\| = \boldsymbol{O}(\|\sum_{t=0}^{k_s} z_t z_t^\mathsf{T}\|) = \boldsymbol{O}(k_s^3). \quad (81)$$

By (81), one can always find a group of $\beta_1, \beta_2 \in \mathbb{R}^+$, such that $\beta_1 k_s^3 I_n \preceq X X^\mathsf{T} \preceq \beta_2 k_s^3 I_n$. In turn, the inverse matrix of $X X^\mathsf{T}$ satisfies

$$\frac{I_n}{\beta_1 k_s^3} \succeq (X X^\mathsf{T})^{-1} \succeq \frac{I_n}{\beta_1 k_s^3}, \tag{82}$$

where the invertibility of $X X^\mathsf{T}$ is guaranteed by the i.i.d. noise $\{\omega_k\}_{k=0}^{k_s}$. Therefore, the spectral norm of $X X^\mathsf{T}$ is characterized by

$$\|(X X^\mathsf{T})^{-1}\| = \boldsymbol{O}(\frac{1}{k_s^3}). \tag{83}$$

- *Part 2: Upper Bounding $\|\Omega_H^+ - W_{HF} \Omega_F^- X^\mathsf{T}\|$.*

Utilizing the concentration measure in Gaussian space [61], given a random matrix $\Omega \in \mathbb{R}^{n_h \times k_s}$ with independent standard normal entries, one has with probability at least $1 - 2\exp\{-r^2/2\}$

$$\|\Omega\| \le \sqrt{k_s} + \sqrt{n} + r. \tag{84}$$

Let $r = \sqrt{2(k_s + n)}$ and utilize $\sqrt{k_s} + \sqrt{n} \le \sqrt{2(k_s + n)}$, one has with probability at least $1 - 2\exp\left(-(k_s + n)\right)$ that $\|\Omega\| \le 2\sqrt{2(k_s + n)}\sigma$. Note that the observation matrix X contains the noise matrix Ω_F^-, i.e., $\mathrm{Exp}[\Omega_F^- X^\mathsf{T}] = \sigma^2 I_{n_f}$. Therefore, it yields that with probability at least $P_3(k_s) = 1 - 2\exp\left\{-(k_s + n_h)\right\}$

$$\|\Omega_H^+ - W_{HF} \Omega_F^- X^\mathsf{T}\| = \boldsymbol{O}(\sigma k_s^2) + \boldsymbol{o}(\sigma^2 k_s). \tag{85}$$

- *Part 3: Upper Bounding $\|(W_{HH} - I_{n_h}) U_\Delta X^\mathsf{T}\|$.*

Recall that $u_\Delta = \hat{h}^H + \hat{c}\mathbb{I}^H$, it can be split as

$$U_\Delta = U_\Delta^c + U_\Delta^h, \tag{86}$$

where $U_\Delta^c = [(\hat{c} - c)\mathbb{I}^H, \cdots, (\hat{c} - c)\mathbb{I}^H]$ and $U_\Delta^H = [\hat{h}^H - h, \cdots, \hat{h}^H - h]$. Then, the upper bound of $\|(U_\Delta + \Omega_H^+) X^\mathsf{T}\|$ is given by

$$\|(U_\Delta + \Omega_H^+) X^\mathsf{T}\| \le \|U_\Delta^c X^\mathsf{T}\| + \|U_\Delta^h X^\mathsf{T}\| + \|\Omega_H^+ X^\mathsf{T}\|. \tag{87}$$

By the conclusion of Theorem 1, with probability at least $P_1(L_c) = 1 - 2\exp\{-\frac{n_f L_c \epsilon^2}{\sigma^2}\}$, one has $\|U_\Delta^c\| \le 4\epsilon \sqrt{n_f k_s / L_c}$ and

$$\|U_\Delta^c X^\mathsf{T}\| = \boldsymbol{O}(\frac{\epsilon k_s^2}{\sqrt{L_c}}). \tag{88}$$

Note that Theorem 1 demonstrates that each term in U_Δ^h is a random variable of ϵ-level mean and σ^2-level variance, and thus one deduces that with probability at least $P_3(k_s)$

$$\|U_\Delta^h X^\mathsf{T}\| = \boldsymbol{O}(\epsilon k_s^2) + \boldsymbol{O}(\sigma k_s^2). \tag{89}$$

Combining (88) and (89), one obtains

$$\|U_\Delta X^\mathsf{T}\| = \boldsymbol{O}(\epsilon k_s^2) + \boldsymbol{O}(\sigma k_s^2). \tag{90}$$

Finally, multiplying the terms (85) and (90) with (83), one has with probability at least $P_1(L_c) \cdot P_3(k_s)$

$$\|\hat{W}_{HF} - W_{HF}\| = \boldsymbol{O}(\frac{\epsilon}{k_s \sqrt{L_c}}) + \boldsymbol{O}(\frac{\epsilon}{k_s}) + \boldsymbol{O}(\frac{\sigma}{k_s}) + \boldsymbol{o}(\frac{\sigma^2}{k_s^2}). \tag{91}$$

Taking ϵ, σ and L_c as fixed constants, (91) can be further characterized as $\|\hat{W}_{HF} - W_{HF}\| = \boldsymbol{O}(\frac{1}{k_s}) + \boldsymbol{o}(\frac{1}{k_s^2})$. The proof is completed. $\qquad\square$

D. Proof of Theorem 5

Proof. To begin with, suppose $R_c \ge \hat{R}_{c1} \ge \hat{R}_{c2}$ and the observations are noise-free for ease notation. Denote by $\mathcal{V}_{F_2}$ the robot set that is within the range $R_{h0} + \hat{R}_{c2}$, and define $\mathcal{N}_{H_0}^{in} = \{j : j \in \mathcal{V}_F, i \in \mathcal{V}_{H_0}, w_{ij} > 0\}$. Then, the filtered observations of $\mathcal{V}_{H_0}$ satisfy

$$Y_{H_0} = W_{H_0 F_2} X_{F_2} + W_{H_0 F_2'} X_{F_2'}, \tag{92}$$

where $\mathcal{V}_{F_2'} = \{\mathcal{N}_{H_0}^{in}\} \cap \{\mathcal{V}_F \backslash \mathcal{V}_{F_2}\}$. Note that $W_{H_0 F_2'} X_{F_2'}$ is a $|\mathcal{V}_{H_0}|$-dimension vector. There exists at least a $|\mathcal{V}_{H_0}| \times |\mathcal{V}_{F_2}|$-dimension matrix $W_{\Delta_0 F_2}$, such that

$$W_{\Delta_0 F_2} Y_{F_2} = W_{H_0 F_2'} X_{F_2'}. \tag{93}$$

Then, substitute (93) into (92) and it yields

$$Y_{H_0} = (W_{H_0 F_2} + W_{\Delta_0 F_2}) X_{F_2}. \tag{94}$$

Taking the observation noises into account, the OLS estimator of $W_{H_0 F_0}(\hat{R}_{c2})$ with observations Y_{H_0} and X_{F_2} is given by

$$\hat{W}_{H_0 F_2}(\hat{R}_{c2}) = Y_{H_0} X_{F_2}^\mathsf{T} (X_{F_2} X_{F_2}^\mathsf{T})^{-1}. \tag{95}$$

Next, applying Theorem 4 on $\hat{W}_{H_0 F_2}(\hat{R}_c)$, it yields that

$$\Pr\{\|\lim_{k_s \to \infty} \hat{W}_{H_0 F_2}(\hat{R}_c) - W_{H_0 F_2}\| = \|W_{\Delta_0 F_2}\|\} = 1. \tag{96}$$

It is straightforward to infer that, if some in-neighbors of $\mathcal{V}_{H_0}$ are in $\mathcal{V}_{F_2'}$, then $\|W_{\Delta_0 F_2}\| > 0$. Therefore, for the local topology estimator $\hat{W}_{H_0 F}(\hat{R}_{c2})$, the asymptotic inference bias is given by

$$f_w(\hat{R}_{c2}) = \left\|\left[W_{\Delta_0 F_2}, W_{H_0 F_2'}\right]\right\|. \tag{97}$$

For $\hat{R}_{c1} \ge \hat{R}_{c2}$, the cardinal numbers of $\mathcal{V}_{F_1'}$ and $\mathcal{V}_{F_2'}$ satisfy $|\mathcal{V}_{F_1'}| \le |\mathcal{V}_{F_2'}|$, which indicates that $\hat{W}_{H_0 F}(\hat{R}_{c1})$ is less biased from the real $W_{H_0 F}$. The monotone decreasing property of $f_w(\hat{R}_c)$ is proved.

Specifically, if $\hat{R}_{c2} \ge R_c$, the set $\mathcal{V}_{F_2'} = \{\mathcal{N}_{H_0}^{in}\} \cap \{\mathcal{V}_F \backslash \mathcal{V}_{F_2}\} = \emptyset$. Finally, it follows that $|\mathcal{V}_{F_2'}| = 0$ and $f_w(\hat{R}_{c2}) = 0$, i.e., $\hat{W}_{H_0 F}(\hat{R}_c)$ is asymptotically unbiased. The proof is completed. $\qquad\square$

REFERENCES

[1] F. Bullo, J. Cortes, and S. Martinez, *Distributed control of robotic networks: A mathematical approach to motion coordination algorithms.* Princeton University Press, 2009, vol. 27.

[2] R. Olfati-Saber and R. M. Murray, "Consensus problems in networks of agents with switching topology and time-delays," *IEEE Transactions on Automatic Control*, vol. 49, no. 9, pp. 1520–1533, 2004.

[3] K.-K. Oh, M.-C. Park, and H.-S. Ahn, "A survey of multi-agent formation control," *Automatica*, vol. 53, pp. 424–440, 2015.

[4] M. A. Kamel, X. Yu, and Y. Zhang, "Formation control and coordination of multiple unmanned ground vehicles in normal and faulty situations: A review," *Annual Reviews in Control*, vol. 49, pp. 128–144, 2020.

[5] D. Zhang and J. P. Sterbenz, "Analysis of critical node attacks in mobile ad hoc networks," in *2014 6th International Workshop on Reliable Networks Design and Modeling*, 2014, pp. 171–178.

[6] B. L. M. Vásquez and J. Carlo Barca, "Network topology inference in swarm robotics," in *IEEE International Conference on Robotics and Automation (ICRA)*. IEEE, 2018, pp. 7660–7666.

[7] H. Choi, W.-C. Lee, Y. Aafer, F. Fei, Z. Tu, X. Zhang, D. Xu, and X. Xinyan, "Detecting attacks against robotic vehicles: A control invariant approach," in *Proceedings of the 2018 ACM SIGSAC Conference on Computer and Communications Security*. ACM, 2018, pp. 801–816.

This article has been accepted for publication in IEEE Transactions on Automatic Control. This is the author's version which has not been fully edited and content may change prior to final publication. Citation information: DOI 10.1109/TAC.2023.3237484

15

[8] Y. Li, J. He, C. Chen, and X. Guan, "Intelligent physical attack against mobile robots with obstacle-avoidance," *IEEE Transactions on Robotics*, 2022 (early access).

[9] R. A. Licitra, Z. I. Bell, and W. E. Dixon, "Single-agent indirect herding of multiple targets with uncertain dynamics," *IEEE Transactions on Robotics*, vol. 35, no. 4, pp. 847–860, 2019.

[10] J. Li, J. He, Y. Li, and X. Guan, "Unpredictable trajectory design for mobile agents," in *2020 American Control Conference (ACC)*. IEEE, 2020, pp. 1471–1476.

[11] A. Venkitaraman, S. Chatterjee, and B. Wahlberg, "Recursive prediction of graph signals with incoming nodes," in *2020 IEEE International Conference on Acoustics, Speech and Signal Processing (ICASSP)*, 2020, pp. 5565–5569.

[12] Y. Li, H. Wang, J. He, and X. Guan, "Optimal topology recovery scheme for multi-robot formation control," in *IEEE 28th International Symposium on Industrial Electronics (ISIE)*. IEEE, 2019, pp. 1847–1852.

[13] S. Shi, G. Bottegal, and P. M. Van den Hof, "Bayesian topology identification of linear dynamic networks," in *2019 European Control Conference (ECC)*. IEEE, 2019, pp. 2814–2819.

[14] F. Lu, M. Zhong, S. Tang, and M. Maggioni, "Nonparametric inference of interaction laws in systems of agents from trajectory data," *Proceedings of the National Academy of Sciences*, vol. 116, no. 29, pp. 14 424–14 433, 2019.

[15] X. Dong, D. Thanou, M. Rabbat, and P. Frossard, "Learning graphs from data: A signal representation perspective," *IEEE Signal Processing Magazine*, vol. 36, no. 3, pp. 44–63, 2019.

[16] S. Shahrampour and V. M. Preciado, "Topology identification of directed dynamical networks via power spectral analysis," *IEEE Transactions on Automatic Control*, vol. 60, no. 8, pp. 2260–2265, 2014.

[17] S. Hassan-Moghaddam, N. K. Dhingra, and M. R. Jovanović, "Topology identification of undirected consensus networks via sparse inverse covariance estimation," in *2016 IEEE 55th Conference on Decision and Control (CDC)*. IEEE, 2016, pp. 4624–4629.

[18] G. Mateos, S. Segarra, A. G. Marques, and A. Ribeiro, "Connecting the dots: Identifying network structure via graph signal processing," *IEEE Signal Processing Magazine*, vol. 36, no. 3, pp. 16–43, 2019.

[19] A. S. Bazanella, M. Gevers, and J. M. Hendrickx, "Network identification with partial excitation and measurement," in *2019 IEEE 58th Conference on Decision and Control (CDC)*. IEEE, 2019, pp. 5500–5506.

[20] H. J. van Waarde, P. Tesi, and M. K. Camlibel, "Topology identification of heterogeneous networks: Identifiability and reconstruction," *Automatica*, vol. 123, p. 109331, 2021.

[21] V. Matta and A. H. Sayed, "Consistent tomography under partial observations over adaptive networks," *IEEE Transactions on Information Theory*, vol. 65, no. 1, pp. 622–646, 2019.

[22] M. Coutino, E. Isufi, T. Maehara, and G. Leus, "State-space network topology identification from partial observations," *IEEE Transactions on Signal and Information Processing over Networks*, vol. 6, pp. 211–225, 2020.

[23] C. Liu, J. He, S. Zhu, and C. Chen, "Dynamic topology inference via external observation for multi-robot formation control," in *2019 IEEE Pacific Rim Conference on Communications, Computers and Signal Processing (PACRIM)*, 2019, pp. 1–6.

[24] Y. Li, J. He, and C. Lin, "Topology inference on partially observable mobile robotic networks under formation control," in *2021 European Control Conference (ECC)*. IEEE, 2021, pp. 497–502.

[25] C. W. Reynolds, "Flocks, herds and schools: A distributed behavioral model," in *Proceedings of the 14th Annual Conference on Computer Graphics and Interactive Techniques*, 1987, pp. 25–34.

[26] X. Sun and C. G. Cassandras, "Optimal dynamic formation control of multi-agent systems in constrained environments," *Automatica*, vol. 73, pp. 169–179, 2016.

[27] S. Zhao, "Affine formation maneuver control of multiagent systems," *IEEE Transactions on Automatic Control*, vol. 63, no. 12, pp. 4140–4155, 2018.

[28] J. Alonso-Mora, E. Montijano, T. Nägeli, O. Hilliges, M. Schwager, and D. Rus, "Distributed multi-robot formation control in dynamic environments," *Autonomous Robots*, vol. 43, no. 5, pp. 1079–1100, 2019.

[29] M. Deghat, I. Shames, B. D. O. Anderson, and C. Yu, "Localization and circumnavigation of a slowly moving target using bearing measurements," *IEEE Transactions on Automatic Control*, vol. 59, no. 8, pp. 2182–2188, 2014.

[30] T.-H. Cheng, Z. Kan, J. R. Klotz, J. M. Shea, and W. E. Dixon, "Event-triggered control of multiagent systems for fixed and time-varying network topologies," *IEEE Transactions on Automatic Control*, vol. 62, no. 10, pp. 5365–5371, 2017.

[31] M. H. Trinh, S. Zhao, Z. Sun, D. Zelazo, B. D. O. Anderson, and H.-S. Ahn, "Bearing-based formation control of a group of agents with leader-first follower structure," *IEEE Transactions on Automatic Control*, vol. 64, no. 2, pp. 598–613, 2018.

[32] S. Zhao, Z. Li, and Z. Ding, "Bearing-only formation tracking control of multiagent systems," *IEEE Transactions on Automatic Control*, vol. 64, no. 11, pp. 4541–4554, 2019.

[33] C. W. Granger, "Investigating causal relations by econometric models and cross-spectral methods," *Econometrica: Journal of the Econometric Society*, pp. 424–438, 1969.

[34] A. Brovelli, M. Ding, A. Ledberg, Y. Chen, R. Nakamura, and S. L. Bressler, "Beta oscillations in a large-scale sensorimotor cortical network: Directional influences revealed by Granger causality," *Proceedings of the National Academy of Sciences*, vol. 101, no. 26, pp. 9849–9854, 2004.

[35] M. Timme, "Revealing network connectivity from response dynamics," *Physical Review Letters*, vol. 98, no. 22, p. 224101, 2007.

[36] W.-X. Wang, Y.-C. Lai, C. Grebogi, and J. Ye, "Network reconstruction based on evolutionary-game data via compressive sensing," *Physical Review X*, vol. 1, no. 2, p. 021021, 2011.

[37] D. Hayden, Y. H. Chang, J. Goncalves, and C. J. Tomlin, "Sparse network identifiability via compressed sensing," *Automatica*, vol. 68, pp. 9–17, 2016.

[38] H.-T. Wai, A. Scaglione, B. Barzel, and A. Leshem, "Joint network topology and dynamics recovery from perturbed stationary points," *IEEE Transactions on Signal Processing*, vol. 67, no. 17, pp. 4582–4596, 2019.

[39] J. Mei and J. M. Moura, "Signal processing on graphs: Modeling (causal) relations in big data," *arXiv preprint arXiv:1503.00173*, vol. 1, 2015.

[40] M. Onuki, S. Ono, M. Yamagishi, and Y. Tanaka, "Graph signal denoising via trilateral filter on graph spectral domain," *IEEE Transactions on Signal and Information Processing over Networks*, vol. 2, no. 2, pp. 137–148, 2016.

[41] H. E. Egilmez, E. Pavez, and A. Ortega, "Graph learning from data under Laplacian and structural constraints," *IEEE Journal of Selected Topics in Signal Processing*, vol. 11, no. 6, pp. 825–841, 2017.

[42] D. Hallac, Y. Park, S. Boyd, and J. Leskovec, "Network inference via the time-varying graphical lasso," in *Proceedings of the 23rd ACM SIGKDD International Conference on Knowledge Discovery and Data Mining*. ACM, 2017, pp. 205–213.

[43] B. Pasdeloup, V. Gripon, G. Mercier, D. Pastor, and M. G. Rabbat, "Characterization and inference of graph diffusion processes from observations of stationary signals," *IEEE Transactions on Signal and Information Processing over Networks*, vol. 4, no. 3, pp. 481–496, 2018.

[44] G. Karanikolas, G. B. Giannakis, K. Slavakis, and R. M. Leahy, "Multi-kernel based nonlinear models for connectivity identification of brain networks," in *2016 IEEE International Conference on Acoustics, Speech and Signal Processing (ICASSP)*. IEEE, 2016, pp. 6315–6319.

[45] G. V. Karanikolas, O. Sporns, and G. B. Giannakis, "Multi-kernel change detection for dynamic functional connectivity graphs," in *2017 51st Asilomar Conference on Signals, Systems, and Computers*. IEEE, 2017, pp. 1555–1559.

[46] S. Wang, E. D. Herzog, I. Z. Kiss, W. J. Schwartz, G. Bloch, M. Sebek, D. Granados-Fuentes, L. Wang, and J.-S. Li, "Inferring dynamic topology for decoding spatiotemporal structures in complex heterogeneous networks," *Proceedings of the National Academy of Sciences*, vol. 115, no. 37, pp. 9300–9305, 2018.

[47] R. Olfati-Saber, J. A. Fax, and R. M. Murray, "Consensus and cooperation in networked multi-agent systems," *Proceedings of the IEEE*, vol. 95, no. 1, pp. 215–233, 2007.

[48] A. Pandey, S. Pandey, and D. R. Parhi, "Mobile robot navigation and obstacle avoidance techniques: A review," *International Robotics and Automation Journal*, vol. 2, no. 3, pp. 96–105, 2017.

[49] A. Santos, V. Matta, and A. H. Sayed, "Local tomography of large networks under the low-observability regime," *IEEE Transactions on Information Theory*, vol. 66, no. 1, pp. 587–613, 2020.

[50] M. Cirillo, V. Matta, and A. H. Sayed, "Learning Bollobás-Riordan graphs under partial observability," in *2021 IEEE International Conference on Acoustics, Speech and Signal Processing (ICASSP)*. IEEE, 2021, pp. 5360–5364.

[51] A. Carè, B. C. Csáji, M. C. Campi, and E. Weyer, "Finite-sample system identification: An overview and a new correlation method," *IEEE Control Systems Letters*, vol. 2, no. 1, pp. 61–66, 2018.

[52] N. Matni and S. Tu, "A tutorial on concentration bounds for system identification," in *2019 IEEE 58th Conference on Decision and Control (CDC)*, 2019, pp. 3741–3749.

This article has been accepted for publication in IEEE Transactions on Automatic Control. This is the author's version which has not been fully edited and content may change prior to final publication. Citation information: DOI 10.1109/TAC.2023.3237484

16

[53] S. Boyd, S. P. Boyd, and L. Vandenberghe, *Convex optimization*. Cambridge University Press, 2004.

[54] Y. Cao and W. Ren, "Sampled-data discrete-time coordination algorithms for double-integrator dynamics under dynamic directed interaction," *International Journal of Control*, vol. 83, no. 3, pp. 506–515, 2010.

[55] A. Bolstad, B. D. Van Veen, and R. Nowak, "Causal network inference via group sparse regularization," *IEEE Transactions on Signal Processing*, vol. 59, no. 6, pp. 2628–2641, 2011.

[56] A. Venkitaraman and D. Zachariah, "Learning sparse graphs for prediction of multivariate data processes," *IEEE Signal Processing Letters*, vol. 26, no. 3, pp. 495–499, 2019.

[57] R. Tibshirani, "Regression shrinkage and selection via the lasso," *Journal of the Royal Statistical Society: Series B (Methodological)*, vol. 58, no. 1, pp. 267–288, 1996.

[58] S.-J. Kim, K. Koh, M. Lustig, S. Boyd, and D. Gorinevsky, "An interior-point method for large-scale l_1-regularized least squares," *IEEE Journal of Selected Topics in Signal Processing*, vol. 1, no. 4, pp. 606–617, 2007.

[59] Y. Zhu, M. T. Schaub, A. Jadbabaie, and S. Segarra, "Network inference from consensus dynamics with unknown parameters," *IEEE Transactions on Signal and Information Processing over Networks*, vol. 6, pp. 300–315, 2020.

[60] M. J. Wainwright, *High-dimensional statistics: A non-asymptotic viewpoint*. Cambridge University Press, 2019.

[61] K. R. Davidson and S. J. Szarek, "Local operator theory, random matrices and banach spaces," *Handbook of the geometry of Banach spaces*, vol. 1, no. 317-366, p. 131, 2001.

Cai Lin (Fellow, IEEE) received her M.A.Sc. and Ph. D. degrees in electrical and computer engineering from the University of Waterloo, Waterloo, Canada, in 2002 and 2005, respectively. Since 2005, she has been with the Department of Electrical & Computer Engineering at the University of Victoria, and she is currently a Professor. She is an NSERC E.W.R. Steacie Memorial Fellow, an Engineering Institute of Canada (EIC) Fellow, and an IEEE Fellow. In 2020, she was elected as a Member of the Royal Society of Canada's College of New Scholars, Artists and Scientists, and a 2020 "Star in Computer Networking and Communications" by N2Women. Her research interests span several areas in communications and networking, with a focus on network protocol and architecture design supporting emerging multimedia traffic and the Internet of Things. She has co-founded and chaired the IEEE Victoria Section Vehicular Technology and Communications Joint Societies Chapter. She has been elected to serve the IEEE Vehicular Technology Society Board of Governors, 2019 - 2024, and served its VP Mobile Radio, 2023. She has been a voting Board Member of IEEE Women in Engineering (2022-23). She has served as an Associate Editor-in-Chief for IEEE Transactions on Vehicular Technology, a member of the Steering Committee of the IEEE Transactions on Big Data (TBD) and IEEE Transactions on Cloud Computing (TCC), an Associate Editor of the IEEE Internet of Things Journal, IEEE/ACM Transactions on Networking, IEEE Transactions on Wireless Communications, IEEE Transactions on Vehicular Technology, IEEE Transactions on Communications, etc., and as the Distinguished Lecturer of the IEEE VTS Society and the IEEE Communications Society.

Yushan Li (Student Member, IEEE) received the B.E. degree in automatic control from the School of Artificial Intelligence and Automation, Huazhong University of Science and Technology, Wuhan, China, in 2018. He is currently working toward the Ph.D. degree in control science and engineering with the Department of Automation, Shanghai Jiaotong University, Shanghai, China. He is a member of Intelligent of Wireless Networking and Cooperative Control group. His research interests include robotics, security of cyber-physical system, and distributed computation and optimization in multi-agent networks.

Xinping Guan (Fellow, IEEE) received the B.Sc. degree in Mathematics from Harbin Normal University, Harbin, China, in 1986, and the Ph.D. degree in Control Science and Engineering from Harbin Institute of Technology, Harbin, China, in 1999. He is currently a Chair Professor with Shanghai Jiao Tong University, Shanghai, China, where he is the Dean of School of Electronic, Information and Electrical Engineering, and the Director of the Key Laboratory of Systems Control and Information Processing, Ministry of Education of China. Before that, he was the Professor and Dean of Electrical Engineering, Yanshan University, Qinhuangdao, China. Dr. Guan's current research interests include industrial cyber-physical systems, wireless networking and applications in smart factory, and underwater networks. He has authored and/or coauthored 5 research monographs, more than 270 papers in IEEE Transactions and other peer-reviewed journals, and numerous conference papers. As a Principal Investigator, he has finished/been working on many national key projects. He is the leader of the prestigious Innovative Research Team of the National Natural Science Foundation of China (NSFC).

Dr. Guan is an Executive Committee Member of Chinese Automation Association Council and the Chinese Artificial Intelligence Association Council. He received the First Prize of Natural Science Award from the Ministry of Education of China in both 2006 and 2016, and the Second Prize of the National Natural Science Award of China in both 2008 and 2018. He was a recipient of the "IEEE Transactions on Fuzzy Systems Outstanding Paper Award" in 2008. He is a "National Outstanding Youth" honored by NSF of China, "Changjiang Scholar" by the Ministry of Education of China and "State-level Scholar" of "New Century Bai Qianwan Talent Program" of China.

Jianping He (Senior Member, IEEE) is currently an associate professor in the Department of Automation at Shanghai Jiao Tong University. He received the Ph.D. degree in control science and engineering from Zhejiang University, Hangzhou, China, in 2013, and had been a research fellow in the Department of Electrical and Computer Engineering at University of Victoria, Canada, from Dec. 2013 to Mar. 2017. His research interests mainly include the distributed learning, control and optimization, security and privacy in network systems.

Dr. He serves as an Associate Editor for IEEE Trans. Control of Network Systems, IEEE Open Journal of Vehicular Technology, and KSII Trans. Internet and Information Systems. He was also a Guest Editor of IEEE TAC, International Journal of Robust and Nonlinear Control, etc. He was the winner of Outstanding Thesis Award, Chinese Association of Automation, 2015. He received the best paper award from IEEE WCSP'17, the best conference paper award from IEEE PESGM'17, and was a finalist for the best student paper award from IEEE ICCA'17, and the finalist best conference paper award from IEEE VTC'20-FALL.